Molecular Therapy
Nucleic Acids
Original Article

AAV-mediated delivery of osteoblast/osteoclast-regulating miRNAs for osteoporosis therapy

Aijaz Ahmad John,[1] Jun Xie,[2,3,4] Yeon-Suk Yang,[1] Jung-Min Kim,[1] Chujiao Lin,[1] Hong Ma,[2,3,4] Guangping Gao,[2,3,4,5] and Jae-Hyuck Shim[1,2,5]

[1]Department of Medicine, Division of Rheumatology, University of Massachusetts Chan Medical School, Worcester, MA, USA; [2]Horae Gene Therapy Center, University of Massachusetts Chan Medical School, Worcester, MA, USA; [3]Department of Microbiology and Physiological Systems, University of Massachusetts Chan Medical School, Worcester, MA, USA; [4]Viral Vector Core, University of Massachusetts Chan Medical School, Worcester, MA, USA; [5]Li Weibo Institute for Rare Diseases Research, University of Massachusetts Chan Medical School, Worcester, MA, USA

Osteoporosis occurs due to a dysregulation in bone remodeling, a process requiring both bone-forming osteoblasts and bone-resorbing osteoclasts. Current leading osteoporosis therapies suppress osteoclast-mediated bone resorption but show limited therapeutic effects because osteoblast-mediated bone formation decreases concurrently. We developed a gene therapy strategy for osteoporosis that simultaneously promotes bone formation and suppresses bone resorption by targeting two microRNAs (miRNAs)—miR-214-3p and miR-34a-5p. We modulated the expression of these miRNAs using systemically delivered recombinant adeno-associated viral (rAAV) vectors targeting the bone. rAAV-mediated overexpression of miR-214-3p or inhibition of miR-34a-5p in the skeleton resulted in bone loss in adult mice, resembling osteoporotic bones. Conversely, rAAV-mediated inhibition of miR-214-3p or overexpression of miR-34a-5p reversed bone loss in mouse models for postmenopausal and senile osteoporosis by increasing osteoblast-mediated bone formation and decreasing osteoclast-mediated bone resorption. Notably, these mice did not show any apparent pathological phenotypes in non-skeletal tissues. Mechanistically, inhibiting miR-214-3p upregulated activating transcription factor 4 in osteoblasts and phatase and tensin homolog in osteoclasts, while overexpressing miR-34a-5p downregulated Notch1 in osteoblasts and TGF-β-induced factor homeobox 2 in osteoclasts. In summary, bone-targeting rAAV-mediated regulation of miR-214-3p or miR-34a-5p is a promising new approach to treat osteoporosis, while limiting adverse effects in non-skeletal tissues.

INTRODUCTION

Bone remodeling is a complex process that requires precise coupling between bone-forming osteoblast and bone-resorbing osteoclast activities at multiple levels (temporal, spatial, and quantitative). Disruption of this osteoblast/osteoclast coupling results in osteoporosis.[1] Osteoblasts coordinate osteoclast differentiation and bone resorption activity, which primarily occurs through the production of the osteoclast differentiation factor, receptor activator of NF-κB ligand (RANKL), and its decoy receptor, osteoprotegerin (OPG), by osteoclasts.[2] Several candidates have also been implicated as coupling factors that promote osteoblast migration and activation via three distinct pathways: (1) soluble factors released from the bone matrix during bone resorption (e.g., TGF-β1[3] and IGF1[4]), (2) soluble factors secreted from osteoclasts (e.g., semaphorin 3A,[5] sphingosine-1-phosphate,[6] and platelet-derived growth factor-BB[7]), and (3) bidirectional cell-to-cell contact between osteoblasts and osteoclasts (e.g., EphrinB2-EphB4[8]). Ironically, these coupling events limit the effectiveness of current osteoporosis therapies, such as bisphosphonate and anti-RANK antibodies targeting osteoclasts to inhibit bone resorption, since they also reduce osteoblast differentiation for bone formation. Similarly, the ability of intermittent parathyroid hormone (PTH) (teriparatide) to promote osteoblast-mediated bone formation is partially counterbalanced by increased osteoclast-mediated bone resorption.[9–11] Thus, there is an unmet need to develop novel therapeutic agents that can increase bone accrual while limiting any counterbalanced effects by osteoblast-osteoclast coupling.

Recent studies have reported that exosomal microRNAs (miRNAs) also function as coupling factors of osteoblast-osteoclast communication.[12,13] miRNAs are a large family of highly conserved small ∼22 nucleotide noncoding RNAs that repress protein-coding genes via messenger RNA (mRNA) degradation or translational inhibition by binding in a sequence-specific manner to the 3′ untranslated region (3′ UTR) of mRNAs.[14,15] Several miRNAs play roles in bone development, remodeling, and regeneration by regulating osteoblast and

Received 31 March 2022; accepted 8 July 2022;
https://doi.org/10.1016/j.omtn.2022.07.008.

Correspondence: Guangping Gao, Horae Gene Therapy Center, University of Massachusetts Chan Medical School, Worcester, MA, USA.
E-mail: guangping.gao@umassmed.edu
Correspondence: Jae-Hyuck Shim, Department of Medicine, Division of Rheumatology, University of Massachusetts Chan Medical School, Worcester, MA, USA.
E-mail: jaehyuck.shim@umassmed.edu

osteoclast differentiation and/or function. For example, miR-20a, miR-26a, miR-29b, miR-125b, miR-133, miR-135, miR-196a, and miR-637 are mainly involved in regulating osteoblast differentiation, while miR-7b, miR-31, miR-26a, miR-145, miR-148a, miR-186, miR-340, and miR-365 control osteoclast differentiation.[16] In addition to these miRNAs, miR-214-3p and miR-34a-5p control both osteoblast and osteoclast differentiation.[13,17–21] Intriguingly, miR-214-3p levels in the bone were highly upregulated by aging-associated or postmenopausal osteoporosis, while miR-34a-5p levels were downregulated in the same conditions (Figure S1), suggesting their association with osteoporosis. miR-214 directly targets activating transcription factor 4 (ATF4) to inhibit osteoblast differentiation,[17] whereas it targets phosphatase and tensin homolog (Pten) and upregulates the phosphatidylinositol 3-kinase (PI3K) pathway to promote osteoclast differentiation.[18] In addition, exosomal miR-214-3p produced by osteoclasts functions as a coupling factor that suppresses the differentiation of neighboring osteoblasts.[22] Conversely, miR-34a-5p plays a negative role in osteoclast differentiation by targeting RANKL,[19] TGF-β-induced factor homeobox 2 (Tgif2),[20] and hypoxia-inducible factor-1α,[21] which downregulates the OPG/RANK/RANKL and IL-33/Notch1 signaling. On the other hand, elevated levels of miR-34a-5p also promoted osteogenic differentiation of mesenchymal stromal cells upon X-ray irradiation[23] or artesunate treatment.[24] Hence, miR-214-3p or miR-34a-5p that can regulate both osteoblast and osteoclast differentiation are attractive targets for osteoporosis therapy.

Although chemically modified miRNA or anti-miRNA oligonucleotides are widely used for *in vitro* and *in vivo* studies, they still have many practical challenges to advance as *in vivo* gene therapy because they require expensive and proprietary modifications and repeated injections.[25,26] Recent studies have demonstrated that delivery of miRNA or anti-miRNA using the 4.7-kb single-stranded DNA parvovirus adeno-associated virus (AAV) vector can resolve these issues.[27,28] AAV vectors have several advantages that make them attractive for use in gene therapy, including high transduction efficiency, long-term expression of miRNAs or anti-miRNAs, relatively low post-infection immunogenicity in adult mammals, and, importantly, no association with any human diseases.[29,30] Given our previous studies that systemic delivery of rAAV9 serotype in adult mice was effective for the transduction of osteoblasts and osteoclasts residing in the skeleton,[31,32] we developed a novel osteoporosis therapy using rAAV9-mediated modulation of two osteoblast/osteoclast-regulating miRNAs, miR-214-3p and miR-34a-5p. rAAV9-mediated inhibition of endogenous miR-214-3p or overexpression of miR-34a-5p counteracted bone loss in mouse models for aging-associated and postmenopausal osteoporosis by simultaneously promoting osteoblast-mediated bone formation while inhibiting osteoclast-mediated bone resorption. Conversely, overexpression of miR-214-3p or inhibition of miR-34a-5p in healthy mice resulted in low bone mass, resembling osteoporotic mice with upregulation of miR-214-3p and downregulation of miR-34a-5p. Since little to no apparent adverse effects in non-skeletal tissues were observed in AAV-treated mice, rAAV9-mediated modulation of miR-214-3p or miR-34a-5p may be a promising and safe therapeutic strategy to treat osteoporosis.

RESULTS

rAAV9-mediated modulation of miR-214-3p regulates osteoblast and osteoclast differentiation *in vitro*

miR-214-3p has been reported to function in both osteoblasts and osteoclasts by inhibiting osteogenesis and promoting osteoclastogenesis.[17,18,22] Together with elevated levels of miR-214-3p in osteoporotic bones (Figure S1A), these data implicate miR-214-3p as a causative factor of osteoporosis. To test this hypothesis, we used an rAAV-mediated gene transfer platform that enabled long-term expression of pre-miR-214-3p or inhibition of endogenous miR-214-3p by miRNA tough decoys (TuDs) containing multiple tandem miR-214-3p binding sites.[27,33] For miR-214-3p expression, pre-miR-214-3p was inserted between the chicken β-actin promoter and the *Egfp* reporter gene; to express TuDs, three tandem miR-214-3p TuDs were inserted between the U6 promoter and the *Guassia* luciferase (gLuc) reporter gene to track AAV-transduced cells or tissues (Figures 1A, S2A, and S2B). The AAV vector genome expressing miR-214-3p was validated in HEK293 cells using RT-PCR (Figure 1B). Overexpression of miR-214-3p markedly reduced β-galactosidase activity of the sensor plasmid that contains miR-214-3p-target sequences in the 3′ UTR of the *LacZ* reporter gene (Figure S2C) but did not affect the activity of the control sensor plasmid (Figure 1C). Moreover, the repression of β-galactosidase activity by miR-214-3p was relieved in a dose-dependent manner by adding an AAV vector expressing miR-214-3p TuD (Figure 1D). These results demonstrated that AAV vector genomes can functionally express miR-214-3p or miR-214-3p TuD.

Since the rAAV9 serotype is effective for *in vitro* and *in vivo* transduction of osteoblasts and osteoclasts,[31,32] the test cassettes were then packaged into AAV9 capsids. The *in vitro* transduction efficiency of rAAV9 vector carrying control or miR-214-3p in mouse bone marrow-derived stromal cells (BMSCs) for osteoblast differentiation and bone marrow monocytes (BMMs) for osteoclast differentiation was validated using EGFP expression (Figures S3A and S3B). AAV-mediated overexpression of miR-214-3p in BMSCs decreased alkaline phosphatase (ALP) activity and osteogenic gene expression, including *Bglap* and *Ibsp*, whereas ALP activity and gene expression were upregulated by miR-214-3p TuD (Figures 1E and 1F). These results demonstrated that the expression of miR-214-3p or miR-214-3p TuD by the rAAV9 vector effectively regulated osteoblast differentiation *in vitro*. As miR-214-3p has been reported to target the master transcription factor of osteogenesis ATF4,[34] mRNA levels of *Atf4* in miR-214-3p-expressing BMSCs were markedly reduced (Figure 1G), suggesting that miR-214-3p inhibits osteoblast differentiation via downregulation of ATF4 expression. Conversely, AAV-mediated expression of miR-214-3p in BMMs increased the number of tartrate-resistant acid phosphatase (TRAP)-positive multinucleated osteoclasts (Figures 1H and 1I), as well as osteoclast gene expression, including *Rank* and *Acp5* (Figure 1J). This effect was reversed by the expression of miR-214-3p TuD. Since miR-214-3p targets the 3′ UTR

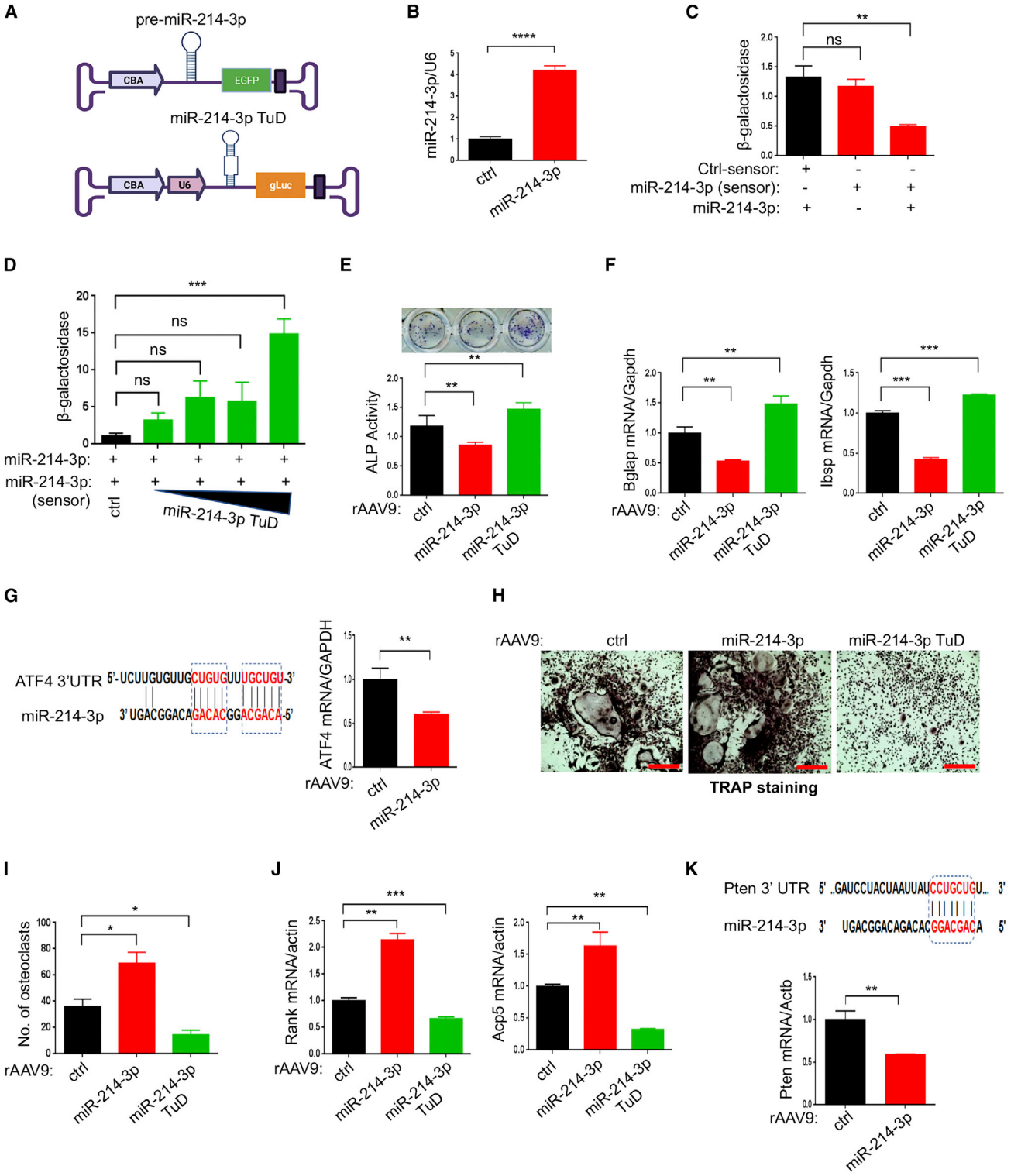

Figure 1. Effects of rAAV9 carrying miR-214-3p or miR-214-3p TuD on osteoblast or osteoclast differentiation

(A) Diagram showing AAV vector genome that contains miR-214-3p and EGFP gene (top) or miR-214-3p TuD and *Guassia* luciferase gene (gLuc, bottom). CBA, CMV enhancer/chicken β-actin promoter. (B) Control (ctrl) or miR-214-3p plasmid was transfected into HEK293 cells and, 48 h later, expression of miR-214-3p was measured by

(legend continued on next page)

of Pten, an inhibitor of RANKL-activated Akt survival signaling,[35] mRNA levels of *Pten* were markedly reduced in miR-214-3p-expressing BMMs (Figure 1K), suggesting that reduced expression of Pten by miR-214-3p promotes osteoclast differentiation due to augmented RANK signaling. Thus, the rAAV9 vector is effective at overexpressing or inhibiting miR-214-3p in both osteoblast and osteoclast progenitors to control osteogenesis and osteoclastogenesis.

rAAV9-mediated modulation of miR-34a-5p regulates osteoblast and osteoclast differentiation *in vitro*

In contrast to miR-214-3p, which decreases osteogenesis and increases osteoclastogenesis, miR-34a-5p increases osteogenesis and decreases osteoclastogenesis,[19,20,24] and its expression was markedly reduced in osteoporotic bones (Figure S1B). To test the possibility that miR-34a-5p inhibits osteoporosis, we constructed the AAV vector genome containing the expression cassette of miR-34a-5p and the *Egfp* reporter gene or miR-34a-5p TuD and *gLuc* reporter gene (Figures 2A, S2A, and S2B). The expression and functional activity of these plasmids in HEK293 cells were validated by RT-PCR (Figure 2B) and by measuring β-galactosidase activity of the sensor plasmid containing miR-34a-5p-target sequences (Figure S2C), respectively. Overexpression of miR-34a-5p markedly reduced β-galactosidase activity (Figure 2C), which was relieved in a dose-dependent manner by expression of miR-34a-5p TuD (Figure 2D). The test cassettes were then packaged into AAV9 capsids, and their transduction efficiency in osteoblasts (BMSCs) and osteoclasts (BMMs) was validated using EGFP expression *in vitro* (Figures S3C and S3D). rAAV9-mediated expression of miR-34a-5p increased osteoblast differentiation, as shown by increased ALP activity and osteogenic gene expression, while osteoblast differentiation was markedly decreased by expression of miR-34a-5p TuD (Figures 2E and 2F), demonstrating a positive role of miR-34a-5p in osteogenesis. Since miR-34a-5p targets Notch1 in pancreatic cancers,[36] mRNA levels of Notch1 were markedly reduced in miR-34a-5p-expressing BMSCs (Figure 2G), suggesting that miR-34a-5p promotes osteoblast differentiation via downregulation of Notch1 expression. Conversely, rAAV9-mediated expression of miR-34a-5p decreased osteoclast differentiation, as shown by a decrease in the number of TRAP-positive multinucleated osteoclasts (Figures 2H and 2I) and osteoclast gene expression (Figure 2J), whereas miR-34a-5p TuD promoted osteoclast differentiation. Since miR-34a-5p targets Tgif2, a key regulator of osteoclast function and differentiation,[20] miR-34a-5p-expressing BMMs showed reduced mRNA levels of *Tgif2* (Figure 2K), suggesting that miR-34a-5p inhibits osteoclast differentiation via downregulation of Tgif2 expression (Figure 2K). Thus, rAAV9-mediated expression of miR-34a-5p or miR-34a-5p TuD is effective in controlling both osteoblast and osteoclast differentiation *in vitro*.

rAAV9-mediated expression of miR-214-3p or miR-34a-5p TuD induces bone loss in mice

To test whether overexpression of miR-214-3p or inhibition of endogenous miR-34a-5p in healthy mice recapitulate bone loss in osteoporotic mice, a single dose of rAAV9 vector carrying control, miR-214-3p, or miR-34a-5p TuD was intravenously (i.v.) injected into 10-week-old mice (Figure 3A). Eight weeks later, expression levels of miR-214-3p and miR-34a-5p in the tibia and serum (Figures 3B and 3E) and femoral bone mass were assessed by RT-PCR and microCT, respectively (Figures 3C, 3D, 3F, and 3G). rAAV9's distribution in individual tissues was examined by EGFP expression using fluorescence microscopy, demonstrating AAV's transduction in the bone, heart, liver, and muscle, but not in the brain (Figure S4B). EGFP-expressing cells were observed in the epiphyseal area of the femur, indicating that i.v. injected rAAV9 vector targets osteoblasts and osteoclasts residing in the bone with high bone remodeling activity (Figure S4B). MicroCT analysis revealed low bone mass in the femurs treated with miR-214-3p or miR-34a-5p TuD relative to control, as demonstrated by a significant decrease in trabecular bone volume/tissue volume (BV/TV), trabecular numbers, and trabecular thickness (Figure 3C, 3D, 3F, and 3G). These results suggest that systemic delivery of the rAAV9 vector effectively expresses miR-214-3p and miR-34a-5p TuD in osteoblast- and osteoclast-lineage cells and results in bone loss *in vivo*.

rAAV9-mediated expression of miR-214-3p TuD or miR-34a-5p counteracts bone loss in postmenopausal osteoporosis

Osteoporosis results in severe bone loss and deterioration of bone architecture, increasing the risk of bone fractures.[37] Bone loss in postmenopausal women mainly results from a lack of estrogen, which is normally produced as a part of the menstrual cycle. It acts on osteoclasts as a negative regulator that prevents osteoclast-mediated bone resorption while promoting bone formation due to augmented osteoblast differentiation.[38] Since rAAV9-mediated expression of miR-214-3p TuD or miR-34a-5p resulted in increased osteogenesis and decreased osteoclastogenesis (Figures 1 and 2), we examined whether systemic delivery of rAAV9 carrying miR-214-3p TuD or miR-34a-5p can promote osteoblast-mediated bone formation and suppress

RT-PCR and normalized to *U6*. (C) HEK293 cells were transfected with ctrl-sensor or miR-214-3p-sensor plasmid in the absence or presence of miR-214-3p plasmid and, 48 h later, β-galactosidase activity was measured and normalized to firefly luciferase. (D) The miR-214-3p plasmid was transfected into HEK293 cells along with the miR-214-3p-sensor plasmid and increasing concentrations of the miR-214-3p TuD plasmid. After 48 h, β-galactosidase activity was measured and normalized to firefly luciferase. (E–G) Mouse bone marrow-derived stromal cells (BMSCs) were transduced with rAAV9 carrying ctrl, miR-214-3p, or miR-214-3p TuD for 2 days and cultured under osteogenic conditions. ALP staining and activity (E) and expression of *Bglap* and *Ibsp* (F) were assessed at day 6 of culture. (G) Computational analysis showing the complementarities of miR-214-3p to the 3′ UTR of *Atf4* (left). mRNA levels of *Atf4* in miR-214-3p-expressing BMSCs were assessed by RT-PCR (right). (H–K) Two days after treatment with M-CSF and RANKL, mouse bone marrow monocytes (BMMs) were transduced with rAAV9 carrying ctrl, miR-214-3p, or miR-214-3p TuD, cultured under osteoclast differentiation conditions, and stained for TRAP. Representative images of TRAP-stained osteoclasts are shown (H), and the number of TRAP-positive osteoclasts assessed (I). mRNA levels of *Rank* and *Acp5* were measured by RT-PCR and normalized to *Actb* (J). (K) The predicted consequential pairing of *Pten* 3′ UTR with miR-214-3p is shown (top) and *Pten* expression as measured by RT-PCR (bottom). Scale bar, 400 μm in (H). Values represent mean ± SD: ns, not significant; *p < 0.05, **p < 0.01, ***p < 0.001, ****p < 0.0001 by an unpaired two-tailed Student's t test (B, G, and K) and one-way ANOVA test (C–F, I, and J).

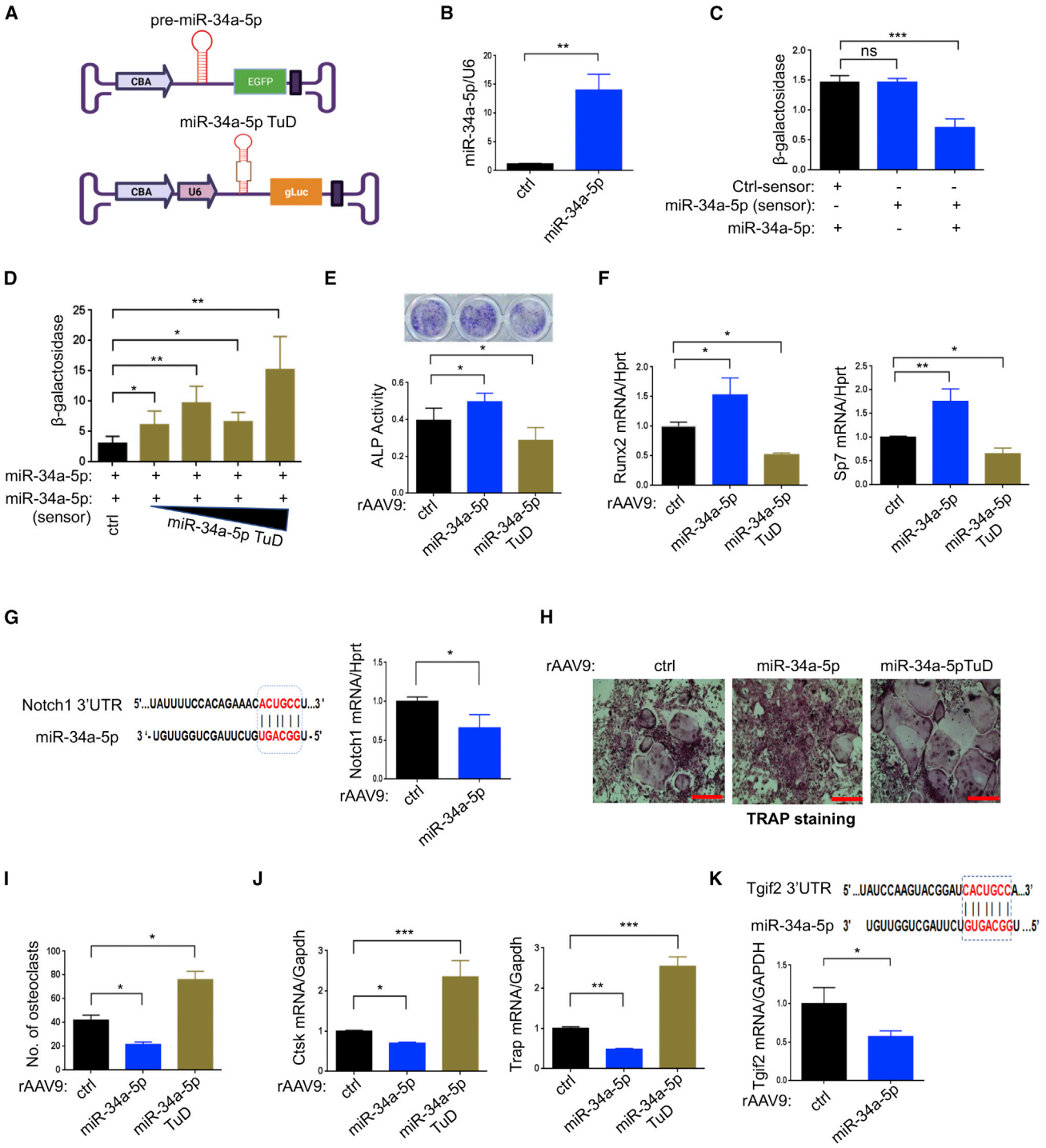

Figure 2. Effects of rAAV9 carrying miR-34a-5p or miR-34a-5p TuD on osteoblast or osteoclast differentiation

(A) Diagram showing AAV vector genome that contains miR-34a-5p and EGFP gene (top) or miR-34a-5p TuD and gLuc reporter gene (bottom). (B) A control (ctrl) or miR-34a-5p plasmid was transfected into HEK293 cells and, 48 h later, expression of miR-34a-5p was measured by RT-PCR and normalized to *U6*. (C) HEK293 cells were transfected with ctrl-sensor or miR-34a-5p-sensor plasmid in the absence or presence of miR-34a-5p plasmid and, 48 h later, β-galactosidase activity was measured and normalized to firefly luciferase. (D) The miR-34a-5p plasmid was transfected into HEK293 cells along with the miR-34a-5p-sensor plasmid with increasing concentrations of miR-34a-5p TuD plasmid. After 48 h, β-galactosidase activity was measured and normalized to firefly luciferase. (E–G) Mouse BMSCs were transduced with rAAV9 carrying ctrl, miR-34a-5p, or miR-34a-5p TuD for 2 days and cultured under osteogenic conditions. ALP staining and activity (E) and expression of *Runx2* and *Sp7* (F) were assessed at day 6 of

(legend continued on next page)

osteoclast-mediated bone resorption in mice, thereby reversing bone loss in postmenopausal osteoporosis.

Ovariectomized (OVX) mice are an established model for postmenopausal osteoporosis induced by estrogen deficiency.[39] Sham or OVX surgery was conducted on 12-week-old female mice, and a single dose of rAAV9 carrying control, miR-214-3p TuD, or miR-34a-5p was i.v. injected 4 weeks post-surgery (Figure 4A). Eight weeks after injection, a reduced expression of endogenous miR-214-3p or increased expression of miR-34a-5p in the tibia was validated by RT-PCR (Figure 4B). While control-treated OVX mice showed a significant decrease in trabecular bone mass relative to sham mice, bone loss was almost completely reversed in the femur of OVX mice treated with miR-214-3p TuD or miR-34a-5p, as shown by increased trabecular BV/TV, thickness, and numbers (Figures 4C and 4G). Likewise, bone formation rate (BFR) and mineral apposition rate (MAR) were markedly increased in these mice, demonstrating augmented osteoblast activity *in vivo* (Figures 4D and 4H). OVX mice treated with miR-214 TuD or miR-34a-5p also displayed a significant decrease in numbers of TRAP-positive osteoclasts and serum levels of C-terminal telopeptide type I collagen (CTX), demonstrating reduced osteoclast differentiation and resorption activity *in vivo*, respectively (Figure 4E, 4F, 4I, and 4J). These results suggest that systemic delivery of rAAV9 carrying miR-214-3p TuD or miR-34a-5p simultaneously promotes osteoblast-mediated bone formation and suppresses osteoclast-mediated bone resorption, thereby effectively counteracting bone loss after the onset of postmenopausal osteoporosis.

rAAV9-mediated expression of miR-214-3p TuD or miR-34a-5p reverses aging-associated osteoporosis

Aging-associated osteoporosis typically occurs after the age of 70 years for both men and women mainly due to senescence of skeletal stem cells and progenitors and deficiency of calcium and vitamin D, resulting in decreased osteoblast activity, increased adipogenesis, and impaired DNA repair.[40] To test the therapeutic effects of rAAV9 carrying miR-214-3p TuD or miR-34a-5p in a mouse model for senile osteoporosis, 24-month-old male mice were i.v. injected with a single dose of rAAV9 carrying control, miR-214-3p TuD, or miR-34a-5p (Figure 5A). Eight weeks later, knockdown of endogenous miR-214-3p or overexpression of miR-34a-5p in the tibia was validated by RT-PCR (Figure 5B). Compared with control-treated mice, miR-214-3p TuD- or miR-34a-5p-treated mice showed a significant increase in trabecular bone mass within the femur, as indicated by increased trabecular BV/TV, thickness, and number (Figures 5C and 5F). While femoral BFR and MAR were substantially increased (Figures 5D and 5G), these mice displayed reduced levels of serum CTX (Figures 5E and 5H). This is accompanied with elevated levels of calcium in the serum (Figure S5A). These results demonstrated that systemic delivery of rAAV9 carrying miR-214-3p TuD or miR-34a-5p is also effective in reversing aging-associated osteoporosis by promoting osteoblast-mediated bone formation and suppressing osteoclast-mediated bone resorption simultaneously. Notably, treatment with miR-214-3p TuD, but not miR-34a-5p, markedly reduced expression of cell senescence genes, including p21 and IL-6, in the tibia (Figures S5B and S5C), suggesting therapeutic potentials of miR-214-3p TuD to reverse both cell senescence and bone loss in aging-associated osteoporosis. Taken together, inhibition of endogenous miR-214-3p or overexpression of miR-34a-5p via rAAV9-mediated delivery to the bone, which simultaneously promotes bone formation and inhibits bone resorption, is a promising therapeutic approach for the treatment of both postmenopausal and aging-associated osteoporosis.

No adverse effects of rAAV9 carrying miR-214-3p TuD or miR-34a-5p in mice

Previous studies have demonstrated that miR-214-3p plays roles in various biological processes, including skeletal development and homeostasis, cancer development, immune responses, skeletal muscle development, ischemic injury in the heart, and angiogenesis,[41] while miR-34a-5p is important for the regulation of multiple target genes involved in cancer cell growth, proliferation, apoptosis, and invasion.[42–44] Given their expression and pleiotropic roles in various tissues, we tested whether rAAV9-mediated inhibition of miR-214-3p or overexpression of miR-34a-5p causes any untoward adverse effects on non-skeletal tissues. A single dose of rAAV9 vectors carrying control, miR-214-3p TuD, or miR-34a-5p was i.v. injected into 2-month-old healthy mice and, 8 weeks later, expression levels of miR-214-3p and miR-34a-5p in rAAV9-transduced tissues, including bone, liver, skeletal muscle, heart, and brain, were validated by RT-PCR (Figure 6A). Consistent with our previous publications,[31,32] i.v. injection of rAAV9 vectors shows the highest transduction efficiency in the liver and the lowest transduction efficiency in the brain. Of note, trabecular BV/TV, thickness, and numbers were all comparable between the femurs treated with control, miR-214-3p TuD, or miR-34a-5p (Figures 6B–6E), suggesting that the effects of miR-214-3p TuD or miR-34a-5p on normal bone remodeling are minimal in healthy mice. Likewise, these mice did not show any histological abnormalities in rAAV9-transduced non-skeletal tissues (Figure 6F). Finally, glucose and hemoglobulin levels and numbers of red blood cells, white blood cells, lymphocytes, monocytes, and platelets in the blood were all normal in AAV-treated mice (Figure S6). These results suggest that rAAV9-mediated inhibition of miR-214-3p or overexpression of miR-34a-5p are effective for bone accrual under

culture. (G) Computational analysis showing the complementarities of miR-34a-5p to the 3′ UTR of *Notch1* (left). mRNA levels of *Notch1* in miR-34a-5p-expressing BMSCs were assessed by RT-PCR (right). (H–K) Two days after treatment with M-CSF and RANKL, BMMs were transduced with rAAV9 carrying ctrl, miR-34a-5p, or miR-34a-5p TuD, cultured under osteoclast differentiation conditions, and stained for TRAP. Representative images of TRAP-stained osteoclasts (H) and numbers of TRAP-positive osteoclasts were quantitated (I). mRNA levels of *Ctsk* and *Trap* were measured by RT-PCR and normalized to *Gapdh* (J). (K) The predicted consequential pairing of *Tgif2* 3′ UTR with miR-34a-5p is shown (top) and *Tgif2* expression as measured by RT-PCR (bottom). Scale bar, 400 μm in (H). Values represent mean ± SD: ns, not significant; *p < 0.05, **p < 0.01, ***p < 0.001, ****p < 0.0001 by an unpaired two-tailed Student's t test (B, G, and K) and one-way ANOVA test (C–F, I, and J).

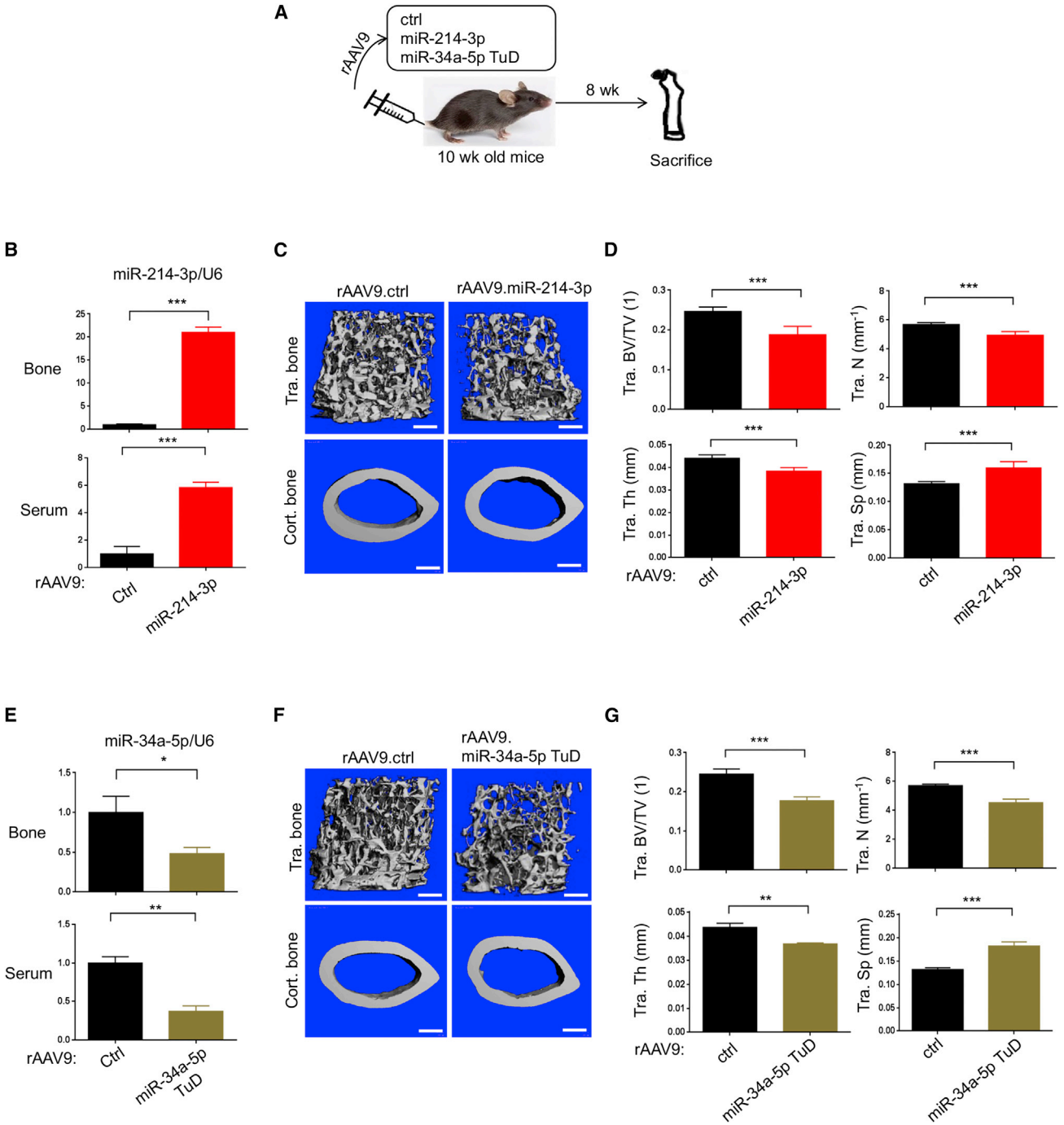

Figure 3. Systemic delivery of rAAV9 carrying miR-214-3p or miR-34a-5p TuD results in low bone mass in mice

(A) Diagram of the study and treatment methods. Ten-week-old healthy mice were i.v. injected with rAAV9 (5×10^{13} kg/vg) carrying ctrl, miR-214-3p, or miR-34a-5p TuD and, 8 weeks later, skeletal analysis was performed. (B and E) Expression of miR-214-3p (B) or miR-34a-5p (E) in the tibia and serum was measured by RT-PCR and normalized to U6 (n = 5). (C, D, F, and G) Femoral bone mass was assessed by microCT. Representative 3D reconstruction (C and F) and relative quantification (D and G) are displayed (n = 5). Tra. BV.TV, trabecular bone volume/total volume; Tra. Th, trabecular thickness; Tra. N, trabecular number per cubic millimeter; Tra. Sp, trabecular space. Scale bars, 400 μm in (C and F). Values represent mean ± SD: *p < 0.05, **p < 0.01, ***p < 0.001 by an unpaired two-tailed Student's t test.

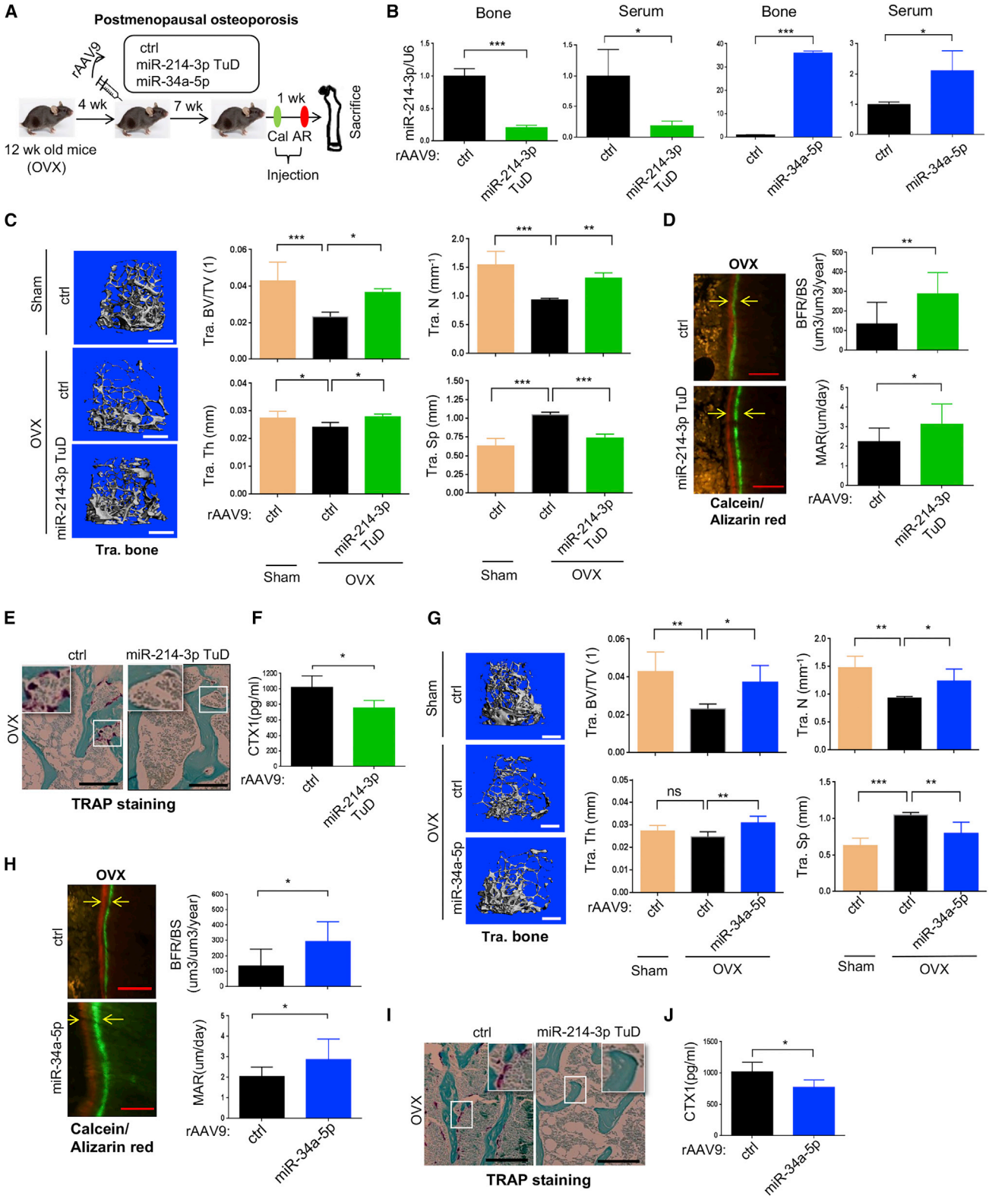

(legend on next page)

pathological conditions and do not affect normal bone homeostasis and non-skeletal tissues.

DISCUSSION

Osteoporosis remains one of the most challenging areas of drug development due in part to a low tolerance for toxicity, the expense of antibody-based biologics, the high burden of taking a long-term medication, and low rates of both physicians appropriately prescribing osteoporosis therapies and patient compliance.[45] Moreover, most existing therapeutic agents for osteoporosis inhibit osteoclast-mediated bone resorption, which is accompanied by numerous potential side effects, including atypical fractures and osteonecrosis of the jaw.[46] Anabolic agents that promote osteoblast function, including intermittent PTH, PTH-related protein, and anti-sclerostin antibody, are also available to treat patients with osteoporosis, but these agents are limited in use due to the fear of bone tumors and untoward cardiovascular events.[9,10,47] Of note, long-term treatment with anti-resorptive drugs also reduces osteoblast function, while the ability of PTH-induced bone formation is counterbalanced by increased osteoclast activity.[9,10] Recently, osteoporosis therapies using AAV-mediated gene transfer have emerged as one of the most promising candidates to address these issues, as they have a clinical track record of being well tolerated and have the potential to efficiently mediate genetic modifications that can persist for years after a single treatment.[29,30,48] In this study, we demonstrated that rAAV9-mediated gene therapy is a complementary approach to traditional osteoporosis drugs, offering the potential ability to deliver long-lasting targeting of previously undruggable intracellular non-enzymatic targets, miRNAs. With a single systemic administration, rAAV9 carrying a bifunctional miRNA (miR-34a-5p) or anti-miRNA (miR-214-3p TuD) in osteoblasts and osteoclasts can almost completely reverse bone loss in both postmenopausal and senile osteoporosis while limiting untoward side effects in non-skeletal tissues.

The therapeutic potential of miRNAs for various metabolic disorders has been demonstrated in multiple pre-clinical studies and human clinical trials.[49] Several miRNAs have been identified as key regulators of osteoblast and/or osteoclast biology and could be used to treat osteoporosis.[13,16,17,24] However, there are still many practical challenges in using these miRNAs, including the requirement of expensive and proprietary modifications and systemic and repeated injection.[25,26] To resolve these issues, we utilized the rAAV9 vector, which is optimized for high transduction efficiency in both osteoblasts and osteoclasts *in vitro* and *in vivo*[31,32] and for long-term expression of miRNA or anti-miRNA.[50,51] In addition, to maximize the therapeutic effectiveness in osteoporosis, a bifunctional miRNA (miR-34a-5p) or anti-miRNA (miR-214-3p TuD) regulating both osteoblast and osteoclast differentiation was delivered to the skeleton via systemically injected rAAV9 vector, which promotes osteoblast-mediated bone formation and inhibits osteoclast-mediated bone resorption simultaneously. Remarkably, as miR-214-3p is upregulated and miR-34a-5p is downregulated under osteoporotic conditions, rAAV9-mediated inhibition of endogenous miR-214-3p and overexpression of miR-34a-5p in osteoblasts and osteoclasts were both effective in counteracting bone loss in mouse models for postmenopausal and senile osteoporosis. Of note, tissue morphology and structure of non-skeletal tissues in AAV-treated mice are largely normal, suggesting little to no obvious anatomic off-target side effects of rAAV9 carrying miR-214-3p TuD or miR-34a-5p. Further studies will be necessary to warrant long-term durability and safety of miRNA expression via rAAV9-mediated delivery. Unlike current therapeutic agents for osteoporosis showing numerous potential side effects and limited therapeutic effectiveness due to counterbalanced coupling events between osteoblasts and osteoclasts, inhibition of miR-214-3p or overexpression of miR-34a-5p via a single systemic administration of rAAV9 vector not only maximizes bone accrual capacity in osteoporosis by controlling osteoblast and osteoclast differentiation simultaneously but also minimizes untoward adverse effects in non-skeletal tissues. Moreover, co-injection with rAAV9.miR-214-3p TuD and rAAV9.miR-34a-5p could further increase therapeutic effectiveness in osteoporosis as a combination therapy. However, further development of a single rAAV9 vector carrying both miRNAs will be necessary to minimize tissue toxicity and immune responses by increased dose of AAV injection and maximize co-expression of miR-214-3p TuD and miR-34a-5p in the same cells. Therefore, bone-targeting AAV-mediated regulation of miR-214-3p and/or miR-34a-5p is a new promising therapeutic alternative for osteoporosis.

Although many miRNAs control osteoblast and osteoclast function during bone development, remodeling, and regeneration, miR-214-3p and miR-34a-5p are the only bifunctional miRNAs regulating both osteoblast and osteoclast differentiation, whose expression levels are associated with postmenopausal and senile osteoporosis. Thus, rAAV9-mediated regulation of these miRNAs in both osteoblasts and osteoclasts may be able to maximize therapeutic efficacy in osteoporosis by promoting osteoblast-mediated bone formation and osteoclast-mediated bone resorption simultaneously, while minimizing counterbalanced events by osteoblast-osteoclast coupling.

Figure 4. Systemic delivery of rAAV9.miR-214-3p TuD reverses osteoporosis in mice

(A) Diagram of the study and treatment methods. Sham or OVX surgery was performed on 12-week-old female mice and, 4 weeks later, a single dose of rAAV9 (5×10^{13} kg/vg) carrying ctrl or miR-214-3p TuD or miR-34a-5p was i.v. injected. Seven weeks after the injection, mice were injected with calcein/alizarin red (AR) for dynamic histomorphometry analysis. (B) miR-214-3p or miR-34a-5p expression in the tibia and serum was measured by RT-PCR and normalized to U6 (n = 5). (C and G) Femoral bone mass was assessed by microCT. Representative 3D reconstruction and relative quantification are displayed (n = 5). (D and H) Representative images of calcein/AR labeling and relative histomorphometric quantification of bone formation rate (BFR)/bone surface (BS) and mineral apposition rate (MAR) are displayed. Arrows indicate the distance between calcein and AR labeling. (E and I) Representative images of TRAP-stained longitudinal sections of AAV-treated femurs. (F and J) Serum levels of CTX-I in AAV-treated mice were assessed by ELISA (n = 5). Scale bars, 400 μm in (C and G) and 50 μm (D, E, H, and I). Values represent mean ± SD: $^{*}p < 0.05$, $^{**}p < 0.01$, $^{***}p < 0.001$ by an unpaired two-tailed Student's t test (B, D, F, H, and J) and one-way ANOVA test (C and G).

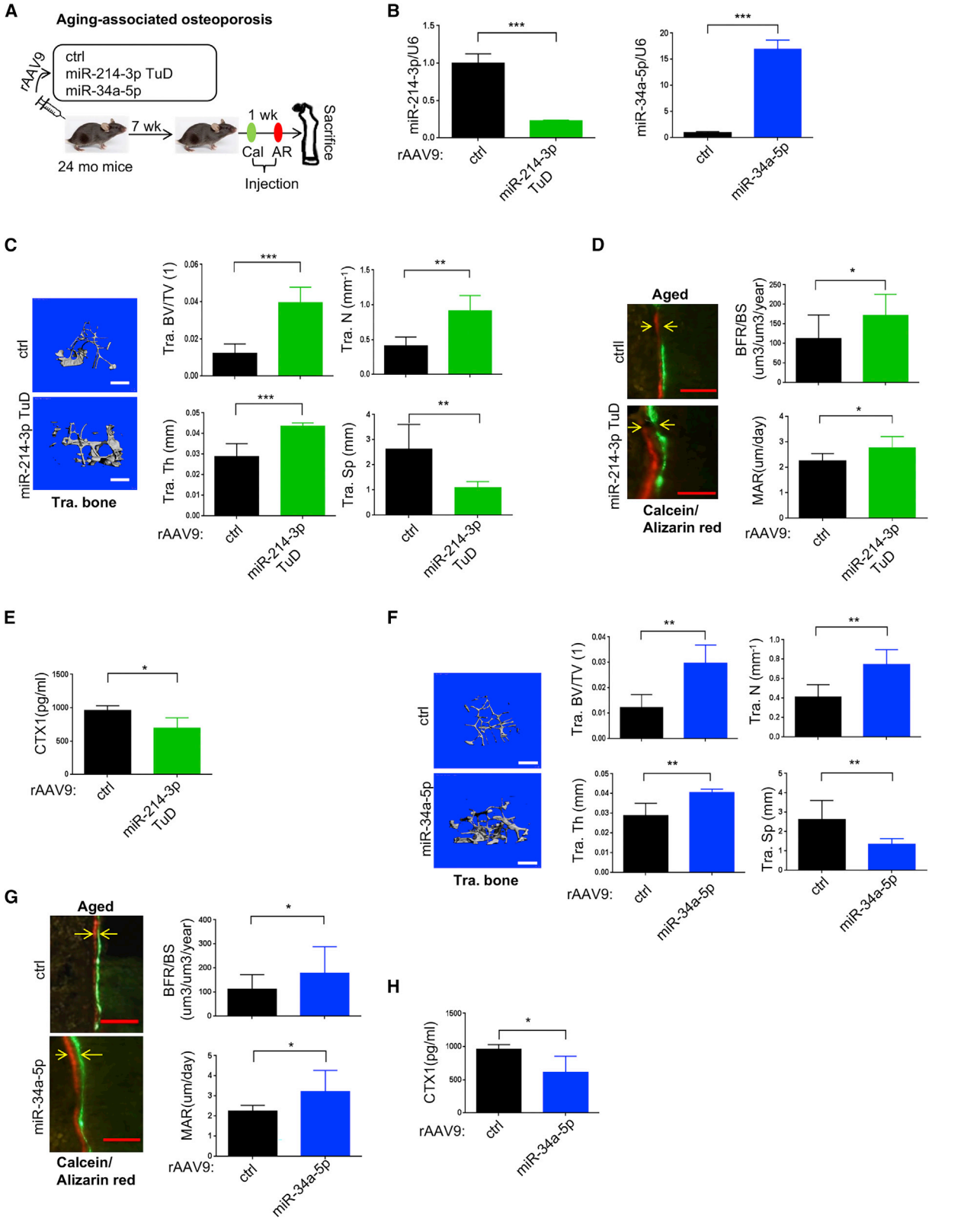

(legend on next page)

Mechanistically, inhibition of endogenous miR-214-3p upregulates the expression of ATF4 in osteoblasts and PTEN in osteoclasts. On the other hand, overexpression of miR-34a-5p downregulates the expression of Notch1 in osteoblasts and Tgif2 in osteoclasts. Although we demonstrate that *Atf4*, *Pten*, *Notch1*, and *Tgif2* are key target genes of miR-214-3p and miR-34a-5p, both miRNAs are likely to have additional target genes that contribute to osteoblast and osteoclast differentiation.

miR-214-3p and miR-34a-5p are also involved in the regulation of T cell function and tumorigenesis. miR-214-3p plays a positive role in T cell proliferation and function by downregulating the expression of Pten, an inhibitor of the PI3K-AKT pathway.[52] Conversely, miR-34a-5p functions as a negative regulator of T cell function by downregulating the expression of the genes associated with the NF-κB signalosome.[53,54] Since activation of T cells under osteoporotic conditions enhances osteoclast-mediated bone resorption,[55] suppression of T cell function by AAV-mediated miR-214-3p inhibition or miR-34a-5p overexpression may contribute to reverse bone loss in osteoporosis. Further studies will be necessary to investigate miRNA's effects on T cell function in osteoporotic mice. Moreover, miR-214-3p and miR-34a-5p have been reported to regulate the progression of various cancers. miR-214-3p acts as an oncogenic factor in gastric, ovarian, and breast cancers that upregulates PI3K/Akt signaling by suppressing Pten expression,[56] while miR-34a-5p is a tumor suppressor of various cancers, including prostate, esophageal, gastric, breast cancers, that inhibits the expression of CD44, FNDC3B, and IGF2BP3.[57] Thus, the potential of AAV-mediated gene therapy modulating miR-214-3p or miR-34a-5p can extend beyond osteoporosis to various cancers.

The ability of miRNAs to regulate multiple target genes may increase untoward side effects; however, it could also improve their therapeutic effectiveness.[58] Other challenges that must be addressed to advance miRNA-based therapeutics include eliminating potential off-target effects and toxicity and guarding against degradation by internal nucleases.[59] These limitations can be addressed by increasing the binding stability and sensitivity of these miRNAs and by protecting them from nuclease degradation via chemical modifications of nucleotides. Future studies are needed to improve cellular uptake and tissue specificity to advance these therapeutics.[25,60–62] We, therefore, utilized the rAAV9 vector that has high transduction efficiency in osteoblasts and osteoclasts and bone-specific tropism. Moreover, future vector modifications can improve the bone-specific tropism of AAV capsid by grafting bone-targeting peptide motifs to the capsid proteins and bone-specific expression using osteoblast or osteoclast-specific promoters, which will allow for even more precise bone-targeting rAAV9 vectors that can deliver miRNA(s) without any non-skeletal adverse effects. Taken together, bone-targeting rAAV9-mediated gene therapy provides a new opportunity to explore miRNA therapeutics for human skeletal disease underlying low bone mass. Moreover, the potential of AAV gene therapy extends beyond osteoporosis, in particular to rare skeletal disorders, where the ability of AAV delivered payloads to correct gene mutations offers one of the only methods that can directly address the genetic defects underlying these disorders.

MATERIALS AND METHODS

AAV vector design, production, and validation

Anti-miR-34a-5p TuD and anti-miR-214-3P TuD were designed and incorporated into pAAVsc.*CB6-Gluc* vector plasmid as described previously.[27] gBlocks containing pre-miR-34a or pre-miR-214 and its ∼100 base pairs flanking sequences at both ends were cloned into the intron of pAAVsc.CB6-EGFP vector plasmid.[32] To monitor the miRNA activity, sensor plasmids were made by inserting three copies of miRNA binding sites after the β-galactosidase reporter gene in the pmiCHECK plasmid.[63] The sequences of oligos and gBlocks for plasmid construction are shown in Table S1. rAAV9 was produced by transient HEK293 cell transfection and CsCl sedimentation at the Viral Vector Core, the University of Massachusetts Chan Medical School, as described previously.[64] Vector preparations were determined by ddPCR, and purity was assessed by 4%–12% SDS-acrylamide gel electrophoresis and silver staining (Invitrogen).

AAV vector genomes expressing miR-214 and miR-34a were transiently transfected into HEK293T cells and, 48 h later, transfection efficiency was examined by EGFP expression using fluorescence microscopy. In addition, miRNA expression was examined by RT-PCR using the TaqMan miRNA assay kit (Applied Biosystems). For functional validation, the AAV vector genomes (500 ng) expressing control, miR-214, or miR-34a were transfected into HEK293T cells along with the sensor plasmids (100 ng) for control (pmiCheck-Scr), miR-214-3p (pmiCheck-miR-214-3p), or miR-34a-5p (pmiCheck-miR-34a-5p). After 48 h, β-galactosidase activity was measured by using Galacto-Star β-Galactosidase Reporter Gene Assay System for Mammalian Cells (Applied Biosystems, T1012) and normalized to firefly luciferase activity (Promega) according to the manufacturer's protocol.

AAV vector genomes expressing miR-214-3p TuD or miR-34a-5p TuD were transfected into HEK293T cells at different concentrations (5, 25, 250, and 500 ng) along with the sensor plasmids (100 ng) for

Figure 5. Systemic delivery of rAAV9 carrying miR-34a-5p reverses osteoporosis in mice

(A) Diagram of the study and treatment methods. 24-month-old male mice were i.v. injected with a single dose of rAAV9 (5×10^{13} kg/vg) carrying ctrl or miR-214-3p TuD or miR-34a-5p and, 7 weeks later, mice were injected with calcein/AR for dynamic histomorphometry analysis. (B) miR-214-3p or miR-34a-5p expression in the tibia was measured by RT-PCR and normalized to U6 (n = 5). (C and F) The femoral bone mass of rAAV-treated mice was assessed by microCT. 3D reconstruction (C and F) (left) and relative quantification (C and F) (right) are displayed (n = 5). (D and G) Representative images of calcein/AR labeling and relative histomorphometric quantification of BFR/BS and MAR are displayed (n = 5). (E and H) Serum levels of CTX-I in AAV-treated mice were assessed by ELISA (n = 5). Scale bars, 50 μm in (D and G). Values represent mean ± SD: *p < 0.05, **p < 0.01, ***p < 0.001, ****p < 0.0001 by an unpaired two-tailed Student's t test.

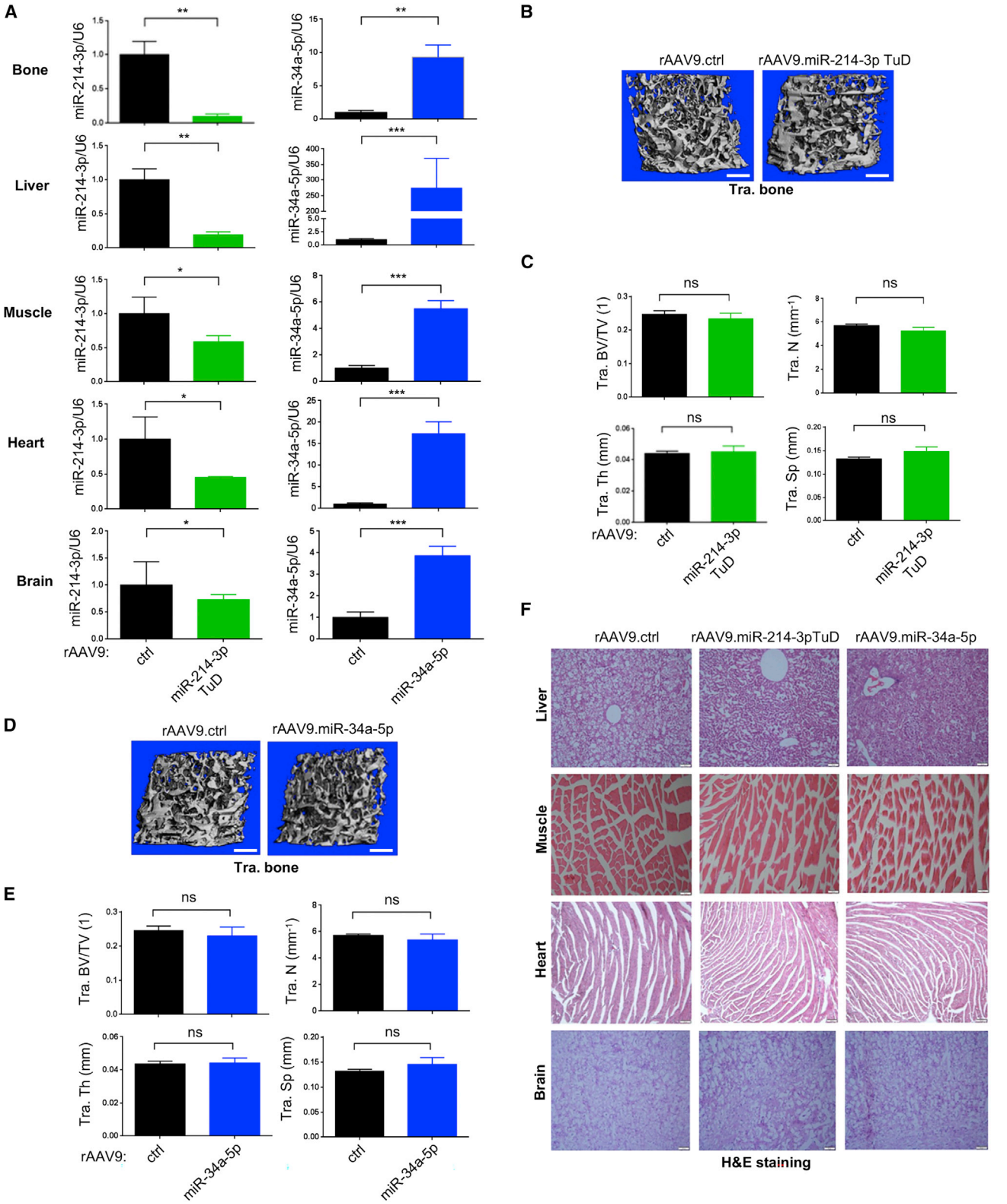

(legend on next page)

control (pmiCheck-Scr), miR-214-3p (pmiCheck-miR-214-3p), or miR-34a-5p (pmiCheck-miR-34a-5p) in presence of AAV vector genomes expressing miR-214-3p or miR-34a-5p, respectively. After 48 h, β-galactosidase activity was measured and normalized to firefly luciferase activity. Details of all DNA plasmids constructs and their gBlock sequences were described in Figure S2 and Table S2.

Cell culture

HEK293T cells were procured from the American Type Culture Collection (Rockville, MD). The cells were grown in DMEM (Corning) supplemented with 10% FBS, 2 mM L-glutamine, 1% penicillin/streptomycin, and 1% nonessential amino acids (all Corning) at 37°C under a humidified atmosphere of 5% CO_2.

Osteoblast and osteoclast culture

For osteoblast culture, BMSCs were harvested from the long bones of 8-week-old wild-type mice (C57BL/6J, Jackson Laboratory). In brief, femurs and tibias were crushed and then, filtered through a 70 μm cell strainer. After treatment with red blood cell lysis buffer, cells were suspended with α-minimal essential medium containing 10% FCS and 1% penicillin/streptomycin (Corning) and cultured in the 60 mm plate at a density of 1×10^7 cells/mL. All non-adherent cells were removed 3 days after the culture. Ascorbic acid (200 μM, Sigma, A8960) and β-glycerophosphate (10 mM, Sigma, G9422) were added to differentiate BMSCs into osteoblasts. BMSCs were seeded at a concentration of 1×10^4 cells/well in a 24-well plate and, 1 day later, cells were incubated with rAAV9 vectors (5×10^{12} GC) for 2 days. To detect osteoblast differentiation, ALP activity was determined as previously described.[65] In brief, differentiated osteoblasts were washed with PBS and incubated with a solution containing 6.5 mM Na_2CO_3, 18.5 mM $NaHCO_3$, 2 mM $MgCl_2$, and phosphatase substrate (Sigma, S0942), and ALP activity was measured using a spectrometer. Alternatively, ALP staining was performed using fast blue (Sigma, FBS25) and Naphthol AS-MX (Sigma, 855) after fixation in 10% neutral formalin buffer.

For the osteoclast differentiation assay, mouse BMMs were harvested from bone marrow cells in the long bones of 8-week-old wild-type mice (C57BL/6J, Jackson Laboratory). In brief, bone marrow cells were flushed out from the femurs and tibias, treated with red blood cell lysis buffer, and suspended with 10% FCS and 1% penicillin/streptomycin (Corning). Cells were cultured in the presence of M-CSF (10 ng/mL, R&D Systems, 416-ML) and, 1 day later, non-adherent cells were plated at a density of 0.5×10^6 cells/well in 24-well plates. BMMs were differentiated into osteoclasts by treatment with M-CSF (10 ng/mL) and RANKL (20 ng/mL, R&D Systems, 462-TEC) and, 2 days later, incubated with rAAV9 vectors (5×10^{12} GC) under osteoclast differentiation conditions for 2 days. To assess osteoclast differentiation, TRAP staining was performed using a leukocyte acid phosphatase staining kit (Sigma, 387A) according to the manufacturer's protocol. The TRAP-stained osteoclasts were detected using an Evos microscope (Applied Biosystems).

Quantitative RT-PCR analysis

A TaqMan microRNA assay kit (Applied Biosystems) was used to measure the expression of miR-214-3p and miR-34a-5p. miRNAs were isolated from tibias, osteoblasts, or osteoclasts using the mirVana miRNA isolation kit (Ambion), followed by cDNA synthesis using the TaqMan miRNA reverse transcription kit (Applied Biosystems). The cDNA was used for RT-PCR using a TaqMan miRNA assay kit (Applied Biosystems) according to the manufacturer's protocol: miR-214-3p (assay ID: 002306), miR-34a-5p (assay ID: 000426), U6 (assay ID: 001973, internal control). Alternatively, total RNA was extracted using QIAzol (QIAGEN), followed by cDNA synthesis using the high-capacity cDNA reverse transcription kit (Applied Biosystems). RT-PCR analysis was performed using SYBR Green PCR master mix (Bio-Rad) with a CFX Connect RT-PCR detection system (Bio-Rad).

miRNA target site prediction

To identify potential target genes for miR-214-3p and miR-34a-5p, two different target prediction tools, i.e., TargetScan (http://www.targetscan.org) and mirdb (http://www.mirdb.org), were used along with a literature survey.

Measurement of crosslinked C-telopeptide of type I collagen

Wild-type serums were harvested from AAV-treated mice by heart puncture after euthanasia and assessed using a C-telopeptide of type I collagen ELISA assay (ABclonal, MC0850).

Serum calcium level measurement

Calcium levels in the serum were assessed using a calcium calorimetric assay kit (Sigma, MAK022) as per the manufacturer's protocol.

Systemic delivery of rAAV9 vectors in healthy and osteoporotic

Wild-type mice were purchased from The Jackson Laboratory (C57BL/6J). Ten-week-old female mice were randomly divided into five groups and injected i.v. via the tail vein with a single dose of rAAV9 vectors (5×10^{13} kg/vg, 200 μL) carrying control, miR-214-3p, miR-214-3p TuD, miR-34a-5p, or miR34a-5p TuD. AAV injection condition was optimized in our previous conditions.[31,32] Eight weeks later, miRNA expression, skeletal analysis, and histopathology

Figure 6. Effects of AAV9 vectors carrying miR-214-3p TuD or miR-34a-5p in healthy mice

(A) 10-week-old mice were i.v. injected with a single dose of rAAV9 (5×10^{13} kg/vg) carrying ctrl, miR-214-3p TuD, or miR-34a-5p and, 8 weeks later, expression of miR-214-3p (left) or miR-34a-5p (right) in the indicated tissues was assessed by RT-PCR (n = 5). (B–E) Femoral bone mass of rAAV-treated mice was assessed by microCT, demonstrating that the AAV treatment had little to no effect on normal bone homeostasis. Representative images of 3D reconstruction (B and D) and relative quantification (C and E) are displayed (n = 5). (F) Representative images of H&E-stained longitudinal sections of the indicated tissues of AAV-treated mice are displayed (n = 5). Scale bars, 400 μm in (B and D) and 100 μm in (F). Values represent mean ± SD: ns, not significant; *p < 0.05, **p < 0.01, ***p < 0.001 by an unpaired two-tailed Student's t test (A, B, and D).

were performed on tibias. For the postmenopausal osteoporosis study, 12-week-old female mice were anesthetized and bilaterally OVX or sham operated. OVX mice were randomly assigned and, 4 weeks later, mice were i.v. injected with a single dose of rAAV9 vectors (5×10^{13} kg/vg, 200 μL) carrying ctrl, miR-214-3p TuD, or miR-34a-5p. Sham mice were i.v. injected with rAAV9 carrying ctrl. Eight weeks later, mice were euthanized, and bone samples were harvested for RT-PCR, microCT, histology, and histomorphometry. For the senile osteoporosis study, 24-month-old female mice were i.v. injected with a single dose of rAAV9 vectors (5×10^{13} kg/vg, 200 μL) carrying ctrl, miR-214-3p TuD, or miR-34a-5p. Eight weeks later, mice were euthanized, and bone samples were harvested for RT-PCR, microCT, histology, and histomorphometry. All animals were used in accordance with the NIH Guide for the Care and Use of Laboratory Animals and were handled according to protocols approved by the University of Massachusetts Chan Medical School Institutional Animal Care and Use Committee.

MicroCT, histology, and histomorphometry analyses

MicroCT was used for qualitative and quantitative assessment of trabecular and cortical bone microarchitecture and performed by an investigator blinded to the genotypes of the animals under analysis, as described previously.[32,65] In brief, femurs dissected from the indicated mice groups were scanned using a microCT 35 (Scanco Medical) with a spatial resolution of 7 μm. For trabecular bone analysis of the distal femur, an upper 2.1 mm region beginning 280 μm proximal to the growth plate was contoured. Three-dimensional reconstruction images were obtained from contoured two-dimensional images by methods based on distance transformation of the binarized images. For cortical bone analysis of the femur, a mid-shaft region of 0.6 mm in length was used. All images presented are representative of the respective genotypes (n = 5).

Histological and histomorphometric analysis was carried out as described previously.[31,32,65] For histological studies, femurs were dissected from AAV-treated mice, fixed in 10% neutral buffered formalin for 2 days, followed by decalcification for 2–4 weeks using 0.5 M tetrasodium EDTA. Further, tissues were dehydrated by passage through an ethanol series, cleared twice in xylene, embedded in paraffin, and sectioned at a thickness of 6 μm along the coronal plate from anterior to posterior. Decalcified femoral sections were stained with TRAP.

For dynamic histomorphometric analysis, mice groups were subcutaneously injected at 6-day intervals with 25 mg/kg calcein (Sigma, C0875) and 50 mg/kg alizarin-3-methyliminodiacetic acid (Sigma, A3882) dissolved in 2% sodium bicarbonate solution. The distances between bone surfaces labeled by calcein (existing bone) and alizarin-3-methyliminodiacetic acid (newly formed bone) were used to assess MARs and mineralized surface/BS to calculate BFRs. After 2 days of fixation in 10% neutral buffered formalin, undecalcified femur samples were embedded in methyl methacrylate, and the proximal metaphyses of femurs were sectioned longitudinally (5 μm) and stained with TRAP for osteoclasts.[66] A region of interest was defined in the trabecular bone of the metaphysis, and BFR/BS and MAR were measured using a Nikon Optiphot 2 microscope interfaced with a semiautomatic analysis system (OsteoMetrics). Measurements were taken on two sections/sample (separated by ~25 μm) and summed before normalization to obtain a single measure/sample in accordance with the American Society of Bone and Mineral Research Histomorphometry Nomenclature Committee.[67] This methodology has undergone extensive quality control and validation, and the results were assessed by two different researchers in a blinded fashion.

Whole-blood glucose level measurement

Whole-blood glucose levels in mice were measured using a handheld whole-blood glucose meter (McKesson) and corresponding glucose test strips. A blood drop was taken by snipping the tip of the tail with sharp scissors, and glucose levels were detected according to the manufacturer's protocol.

Complete blood cell count

Complete blood cell count tests were performed to evaluate cellular components in the blood of AAV-treated mice, including white blood cells, red blood cells, lymphocytes, monocytes, hemoglobin, and platelets. Blood drops were collected into a microtainer EDTA tube and tested within 1 h at room temperature using an automated hematology analyzer (VetScan HM5, Zoetis, USA).

Statistical analysis

Except where indicated, all data are graphically represented as the mean ± SD. For experiments with three or more samples, statistical analysis was performed using one-way ANOVA followed by a Bonferroni-corrected Student's t test. For two-sample comparisons, a two-tailed, unpaired Student's t test was applied. Values were considered statistically significant at $p < 0.05$. Results shown are representative of three or more individual experiments.

DATA AVAILABILITY

Data supporting the findings in this manuscript are available from the corresponding author upon reasonable request.

SUPPLEMENTAL INFORMATION

Supplemental information can be found online at https://doi.org/10.1016/j.omtn.2022.07.008.

ACKNOWLEDGMENTS

We thank Zhihao Chen and Eunhye Son for their technical support. We also thank the many individuals who provided valuable reagents. This project was supported by NIH-NIAMS (R21AR077557 and R01AR078230) and AAVAA Therapeutics. G.G. holds support from grants under the NIH (P01AI100263, R01NS076991, P01HD080642, R01AI12135).

AUTHOR CONTRIBUTIONS

A.A.J. designed, executed, and interpreted the experiments. J.X. and H.M. designed and generated all of the rAAVs used in this work.

Y.-S.Y. performed histology. J.-M.K. performed ovariectomies. G.G. and J.-H.S. supervised the research and prepared the manuscript.

DECLARATION OF INTERESTS

G.G. and J.-H.S. are scientific co-founders of AAVAA Therapeutics and hold equity in this company. G.G. is also a scientific co-founder of Voyager Therapeutics and Aspa Therapeutics and holds equity in these companies. G.G. is an inventor on patents with potential royalties licensed to Voyager Therapeutics, Aspa Therapeutics Inc., and other biopharmaceutical companies.

REFERENCES

1. Harada, S., and Rodan, G.A. (2003). Control of osteoblast function and regulation of bone mass. Nature *423*, 349–355.
2. Trouvin, A.P., and Goeb, V. (2010). Receptor activator of nuclear factor-kappaB ligand and osteoprotegerin: maintaining the balance to prevent bone loss. Clin. Interv. Aging *5*, 345–354.
3. Tang, Y., Wu, X., Lei, W., Pang, L., Wan, C., Shi, Z., Zhao, L., Nagy, T.R., Peng, X., and Hu, J. (2009). TGF-beta1-induced migration of bone mesenchymal stem cells couples bone resorption with formation. Nat. Med. *15*, 757–765.
4. Xian, L., Wu, X., Pang, L., Lou, M., Rosen, C.J., Qiu, T., Crane, J., Frassica, F., Zhang, L., and Rodriguez, J.P. (2012). Matrix IGF-1 maintains bone mass by activation of mTOR in mesenchymal stem cells. Nat. Med. *18*, 1095–1101.
5. Fukuda, T., Takeda, S., Xu, R., Ochi, H., Sunamura, S., Sato, T., Shibata, S., Yoshida, Y., Gu, Z., and Kimura, A. (2013). Sema3A regulates bone-mass accrual through sensory innervations. Nature *497*, 490–493.
6. Ryu, J., Kim, H.J., Chang, E.J., Huang, H., Banno, Y., and Kim, H.H. (2006). Sphingosine 1-phosphate as a regulator of osteoclast differentiation and osteoclast-osteoblast coupling. EMBO. J. *25*, 5840–5851.
7. Xie, H., Cui, Z., Wang, L., Xia, Z., Hu, Y., Xian, L., Li, C., Xie, L., Crane, J., Wan, M., et al. (2014). PDGF-BB secreted by preosteoclasts induces angiogenesis during coupling with osteogenesis. Nat. Med. *20*, 1270–1278.
8. Zhao, C., Irie, N., Takada, Y., Shimoda, K., Miyamoto, T., Nishiwaki, T., Suda, T., and Matsuo, K. (2006). Bidirectional ephrinB2-EphB4 signaling controls bone homeostasis. Cell Metabol. *4*, 111–121.
9. Augustine, M., and Horwitz, M.J. (2013). Parathyroid hormone and parathyroid hormone-related protein analogs as therapies for osteoporosis. Curr. Osteoporos. Rep. *11*, 400–406.
10. Kraenzlin, M.E., and Meier, C. (2011). Parathyroid hormone analogues in the treatment of osteoporosis. Nat. Rev. Endocrinol. *7*, 647–656.
11. Sims, N.A., and Gooi, J.H. (2008). Bone remodeling: multiple cellular interactions required for coupling of bone formation and resorption. Semin. Cell. Dev. Biol. *19*, 444–451.
12. Sun, W., Zhao, C., Li, Y., Wang, L., Nie, G., Peng, J., Wang, A., Zhang, P., Tian, W., Li, Q., et al. (2016). Osteoclast-derived microRNA-containing exosomes selectively inhibit osteoblast activity. Cell Discov. *2*, 16015–16023.
13. Li, D., Liu, J., Guo, B., Liang, C., Dang, L., Lu, C., He, X., Cheung, H.Y.S., Xu, L., Lu, C., et al. (2016). Osteoclast-derived exosomal miR-214-3p inhibits osteoblastic bone formation. Nat. Commun. *7*, 10872.
14. Swarts, D.C., Makarova, K., Wang, Y., Nakanishi, K., Ketting, R.F., Koonin, E.V., Patel, D.J., and Van Der Oost, J. (2014). The evolutionary journey of Argonaute proteins. Nat. Struct. Mol. Biol. *21*, 743–753.
15. Ambros, V. (2003). MicroRNA pathways in flies and worms: growth, death, fat, stress, and timing. Cell *113*, 673–676.
16. Lian, J.B., Stein, G.S., Van Wijnen, A.J., Stein, J.L., Hassan, M.Q., Gaur, T., and Zhang, Y. (2012). MicroRNA control of bone formation and homeostasis. Nat. Rev. Endocrinol. *8*, 212–227.
17. Wang, X., Guo, B., Li, Q., Peng, J., Yang, Z., Wang, A., Li, D., Hou, Z., Lv, K., Kan, G., et al. (2013). miR-214 targets ATF4 to inhibit bone formation. Nat. Med. *19*, 93–100.
18. Zhao, C., Sun, W., Zhang, P., Ling, S., Li, Y., Zhao, D., Peng, J., Wang, A., Li, Q., Song, J., et al. (2015). miR-214 promotes osteoclastogenesis by targeting Pten/PI3k/Akt pathway. RNA Biol. *12*, 343–353.
19. Lopes, H.B., Ferraz, E.P., Almeida, A.L.G., Florio, P., Gimenes, R., Rosa, A.L., and Beloti, M.M. (2016). Participation of MicroRNA-34a and RANKL on bone repair induced by poly (vinylidene-trifluoroethylene)/barium titanate membrane. J. Biomater. Sci. Polym. Ed. *27*, 1369–1379.
20. Peng, W.-X., Ye, C., Dong, W.-T., Yang, L.-L., Wang, C.-Q., Wei, Z.-A., Wu, J.-H., Li, Q., Deng, J., and Zhang, J. (2017). MicroRNA-34a alleviates steroid-induced avascular necrosis of femoral head by targeting Tgif2 through OPG/RANK/RANKL signaling pathway. Exp. Biol. Med. *242*, 1234–1243.
21. Kang, H., Yang, K., Xiao, L., Guo, L., Guo, C., Yan, Y., Qi, J., Wang, F., Ryffel, B., Li, C., and Deng, L. (2017). Osteoblast hypoxia-inducible factor-1α pathway activation restrains osteoclastogenesis via the interleukin-33-MicroRNA-34a-Notch1 pathway. Front. Immunol. *8*, 1312.
22. Li, D., Liu, J., Guo, B., Liang, C., Dang, L., Lu, C., He, X., Cheung, H.Y.-S., Xu, L., Lu, C., et al. (2016). Osteoclast-derived exosomal miR-214-3p inhibits osteoblastic bone formation. Nat. Commun. *7*, 10872–10916.
23. Liu, H., Dong, Y., Feng, X., Li, L., Jiao, Y., Bai, S., Feng, Z., Yu, H., Li, X., and Zhao, Y. (2019). miR-34a promotes bone regeneration in irradiated bone defects by enhancing osteoblastic differentiation of mesenchymal stromal cells in rats. Stem Cell Res. Ther. *10*, 180–214.
24. Zeng, H.-B., Dong, L.-Q., Xu, C., Zhao, X.-H., and Wu, L.-G. (2020). Artesunate promotes osteoblast differentiation through miR-34a/DKK1 axis. Acta. Histochem. *122*, 151601.
25. Krützfeldt, J., Kuwajima, S., Braich, R., Rajeev, K.G., Pena, J., Tuschl, T., Manoharan, M., and Stoffel, M. (2007). Specificity, duplex degradation and subcellular localization of antagomirs. Nucleic. Acids. Res. *35*, 2885–2892.
26. Krützfeldt, J., Rajewsky, N., Braich, R., Rajeev, K.G., Tuschl, T., Manoharan, M., and Stoffel, M. (2005). Silencing of microRNAs in vivo with 'antagomirs. Nature *438*, 685–689.
27. Xie, J., Ameres, S.L., Friedline, R., Hung, J.H., Zhang, Y., Xie, Q., Zhong, L., Su, Q., He, R., Li, M., et al. (2012). Long-term, efficient inhibition of microRNA function in mice using rAAV vectors. Nat. Methods *9*, 403–409.
28. Krol, J., Busskamp, V., Markiewicz, I., Stadler, M.B., Ribi, S., Richter, J., Duebel, J., Bicker, S., Fehling, H.J., Schübeler, D., et al. (2010). Characterizing light-regulated retinal microRNAs reveals rapid turnover as a common property of neuronal microRNAs. Cell *141*, 618–631.
29. Venditti, C.P. (2021). Safety questions for AAV gene therapy. Nat. Biotechnol. *39*, 24–26.
30. Vandenberghe, L.H., Wilson, J.M., and Gao, G. (2009). Tailoring the AAV vector capsid for gene therapy. Gene. Ther. *16*, 311–319.
31. Yang, Y.-S., Xie, J., Wang, D., Kim, J.-M., Tai, P.W.L., Gravallese, E., Gao, G., and Shim, J.-H. (2019). Bone-targeting AAV-mediated silencing of Schnurri-3 prevents bone loss in osteoporosis. Nat. Commun. *10*, 2958–3013.
32. Yang, Y.-S., Xie, J., Chaugule, S., Wang, D., Kim, J.-M., Kim, J., Tai, P.W.L., Seo, S.-K., Gravallese, E., Gao, G., and Shim, J.H. (2020). Bone-targeting AAV-mediated gene silencing in osteoclasts for osteoporosis therapy. Mol. Ther. Methods Clin. Dev. *17*, 922–935.
33. Ebert, M.S., Neilson, J.R., and Sharp, P.A. (2007). MicroRNA sponges: competitive inhibitors of small RNAs in mammalian cells. Nat. Methods *4*, 721–726.
34. Yang, X., Matsuda, K., Bialek, P., Jacquot, S., Masuoka, H.C., Schinke, T., Li, L., Brancorsini, S., Sassone-Corsi, P., Townes, T.M., et al. (2004). ATF4 is a substrate of RSK2 and an essential regulator of osteoblast biology; implication for Coffin-Lowry Syndrome. Cell *117*, 387–398.
35. Sugatani, T., Alvarez, U., and Hruska, K.A. (2003). PTEN regulates RANKL- and osteopontin-stimulated signal transduction during osteoclast differentiation and cell motility. J. Biol. Chem. *278*, 5001–5008.
36. Tang, Y., Tang, Y., and Cheng, Y.S. (2017). miR-34a inhibits pancreatic cancer progression through Snail1-mediated epithelial-mesenchymal transition and the Notch signaling pathway. Sci. Rep. *7*, 38232.

37. Klibanski, A., Adams-Campbell, L., Bassford, T., Blair, S.N., Boden, S.D., Dickersin, K., Gifford, D.R., Glasse, L., Goldring, S.R., and Hruska, K. (2001). Osteoporosis prevention, diagnosis, and therapy. JAMA *285*, 785–795.

38. Nakamura, T., Imai, Y., Matsumoto, T., Sato, S., Takeuchi, K., Igarashi, K., Harada, Y., Azuma, Y., Krust, A., Yamamoto, Y., et al. (2007). Estrogen prevents bone loss via estrogen receptor alpha and induction of Fas ligand in osteoclasts. Cell *130*, 811–823.

39. Bouxsein, M.L., Myers, K.S., Shultz, K.L., Donahue, L.R., Rosen, C.J., and Beamer, W.G. (2005). Ovariectomy-induced bone loss varies among inbred strains of mice. J. Bone. Miner. Res. *20*, 1085–1092.

40. Li, G., Thabane, L., Papaioannou, A., Ioannidis, G., Levine, M.A.H., and Adachi, J.D. (2017). An overview of osteoporosis and frailty in the elderly. BMC. Musculoskelet. Disord. *18*, 46.

41. Amin, M.M.J., Trevelyan, C.J., and Turner, N.A. (2021). MicroRNA-214 in health and disease. Cells *10*, 3274.

42. Liu, C., Kelnar, K., Liu, B., Chen, X., Calhoun-Davis, T., Li, H., Patrawala, L., Yan, H., Jeter, C., Honorio, S., et al. (2011). The microRNA miR-34a inhibits prostate cancer stem cells and metastasis by directly repressing CD44. Nat. Med. *17*, 211–215.

43. Zhou, Y., Huang, T., Siu, H.L., Wong, C.C., Dong, Y., Wu, F., Zhang, B., Wu, W.K.K., Cheng, A.S.L., Yu, J., et al. (2017). IGF2BP3 functions as a potential oncogene and is a crucial target of miR-34a in gastric carcinogenesis. Mol. Cancer *16*, 77.

44. Hong, D.S., Kang, Y.-K., Borad, M., Sachdev, J., Ejadi, S., Lim, H.Y., Brenner, A.J., Park, K., Lee, J.-L., Kim, T.-Y., et al. (2020). Phase 1 study of MRX34, a liposomal miR-34a mimic, in patients with advanced solid tumours. Br. J. Cancer. *122*, 1630–1637.

45. Li, S.-S., He, S.-H., Xie, P.-Y., Li, W., Zhang, X.-X., Li, T.-F., and Li, D.-F. (2021). Recent progresses in the treatment of osteoporosis. Front. Pharmacol. *12*, 717065.

46. Borumandi, F., Aghaloo, T., Cascarini, L., Gaggl, A., and Fasanmade, K. (2015). Antiresorptive drugs and their impact on maxillofacial bone among cancer patients. Anti Cancer Agents Med. Chem. *15*, 736–743.

47. Fabre, S., Funck-Brentano, T., and Cohen-Solal, M. (2020). Anti-sclerostin antibodies in osteoporosis and other bone diseases. J. Clin. Med. *9*, 3439.

48. Smalley, E. (2017). First AAV gene therapy poised for landmark approval. Nat. Biotechnol. *35*, 998–999.

49. Chakraborty, C., Sharma, A.R., Sharma, G., Doss, C.G.P., and Lee, S.-S. (2017). Therapeutic miRNA and siRNA: moving from bench to clinic as next generation medicine. Mol. Ther. Nucleic Acids *8*, 132–143.

50. Duan, Q., Yang, L., Gong, W., Chaugai, S., Wang, F., Chen, C., Wang, P., Zou, M.H., and Wang, D.W. (2015). MicroRNA-214 is upregulated in heart failure patients and suppresses XBP1-mediated endothelial cells angiogenesis. J. Cell. Physiol. *230*, 1964–1973.

51. Kaifer, K.A., Villalón, E., O'Brien, B.S., Sison, S.L., Smith, C.E., Simon, M.E., Marquez, J., O'Day, S., Hopkins, A.E., Neff, R., et al. (2019). AAV9-mediated delivery of miR-23a reduces disease severity in Smn2B/− SMA model mice. Hum. Mol. Genet. *28*, 3199–3210.

52. Yin, Y., Cai, X., Chen, X., Liang, H., Zhang, Y., Li, J., Wang, Z., Chen, X., Zhang, W., Yokoyama, S., et al. (2014). Tumor-secreted miR-214 induces regulatory T cells: a major link between immune evasion and tumor growth. Cell. Res. *24*, 1164–1180.

53. Hart, M., Walch-Rückheim, B., Friedmann, K.S., Rheinheimer, S., Tänzer, T., Glombitza, B., Sester, M., Lenhof, H.P., Hoth, M., Schwarz, E.C., et al. (2019). miR-34a: a new player in the regulation of T cell function by modulation of NF-kappaB signaling. Cell Death Dis. *10*, 46.

54. Hart, M., Walch-Rückheim, B., Krammes, L., Kehl, T., Rheinheimer, S., Tänzer, T., Glombitza, B., Sester, M., Lenhof, H.P., Keller, A., and Meese, E. (2019). miR-34a as hub of T cell regulation networks. J. Immunother. Cancer *7*, 187.

55. Pietschmann, P., Mechtcheriakova, D., Meshcheryakova, A., Föger-Samwald, U., and Ellinger, I. (2016). Immunology of osteoporosis: a mini-review. Gerontology *62*, 128–137.

56. Sharma, T., Hamilton, R., and Mandal, C.C. (2015). miR-214: a potential biomarker and therapeutic for different cancers. Future Oncol. *11*, 349–363.

57. Li, Y., Xia, M., Peng, L., Liu, H., Chen, G., Wang, C., Yuan, D., Liu, Y., and Liu, H. (2021). Downregulation of miR-214-3p attenuates mesangial hypercellularity by targeting PTEN-mediated JNK/c-Jun signaling in IgA nephropathy. Int. J. Biol. Sci. *17*, 3343–3355.

58. Gebert, L.F.R., and MacRae, I.J. (2019). Regulation of microRNA function in animals. Nat. Rev. Mol. Cell. Biol. *20*, 21–37.

59. Ishida, M., and Selaru, F.M. (2013). miRNA-based therapeutic strategies. Curr. Anesthesiol. Rep. *1*, 63–70.

60. Sharma, V.K., and Watts, J.K. (2015). Oligonucleotide therapeutics: chemistry, delivery and clinical progress. Future Med. Chem. *7*, 2221–2242.

61. Bernardo, B.C., Ooi, J.Y.Y., Lin, R.C.Y., and McMullen, J.R. (2015). miRNA therapeutics: a new class of drugs with potential therapeutic applications in the heart. Future Med. Chem. *7*, 1771–1792.

62. Chabot, S., Orio, J., Castanier, R., Bellard, E., Nielsen, S.J., Golzio, M., and Teissié, J. (2012). LNA-based oligonucleotide electrotransfer for miRNA inhibition. Mol. Ther. *20*, 1590–1598.

63. Xie, J., Tai, P.W.L., Brown, A., Gong, S., Zhu, S., Wang, Y., Li, C., Colpan, C., Su, Q., He, R., et al. (2020). Effective and accurate gene silencing by a recombinant AAV-compatible microRNA scaffold. Mol. Ther. *28*, 422–430.

64. Sena-Esteves, M., and Gao, G. (2020). Introducing genes into mammalian cells: viral vectors. Cold Spring Harb. Protoc. *2020*, 095513. pdb. top095513.

65. Kim, J.-M., Yang, Y.-S., Park, K.H., Ge, X., Xu, R., Li, N., Song, M., Chun, H., Bok, S., Charles, J.F., et al. (2020). A RUNX2 stabilization pathway mediates physiologic and pathologic bone formation. Nat. Commun. *11*, 2289–2317.

66. Fukuda, T., Takeda, S., Xu, R., Ochi, H., Sunamura, S., Sato, T., Shibata, S., Yoshida, Y., Gu, Z., Kimura, A., et al. (2013). Sema3A regulates bone-mass accrual through sensory innervations. Nature *497*, 490–493.

67. Parfitt, A.M., Drezner, M.K., Glorieux, F.H., Kanis, J.A., Malluche, H., Meunier, P.J., Ott, S.M., and Recker, R.R. (1987). Bone histomorphometry: standardization of nomenclature, symbols, and units. Report of the ASBMR Histomorphometry Nomenclature Committee. J. Bone. Miner. Res. *2*, 595–610.

OMTN, Volume *29*

Supplemental information

AAV-mediated delivery of osteoblast/osteoclast-regulating miRNAs for osteoporosis therapy

Aijaz Ahmad John, Jun Xie, Yeon-Suk Yang, Jung-Min Kim, Chujiao Lin, Hong Ma, Guangping Gao, and Jae-Hyuck Shim

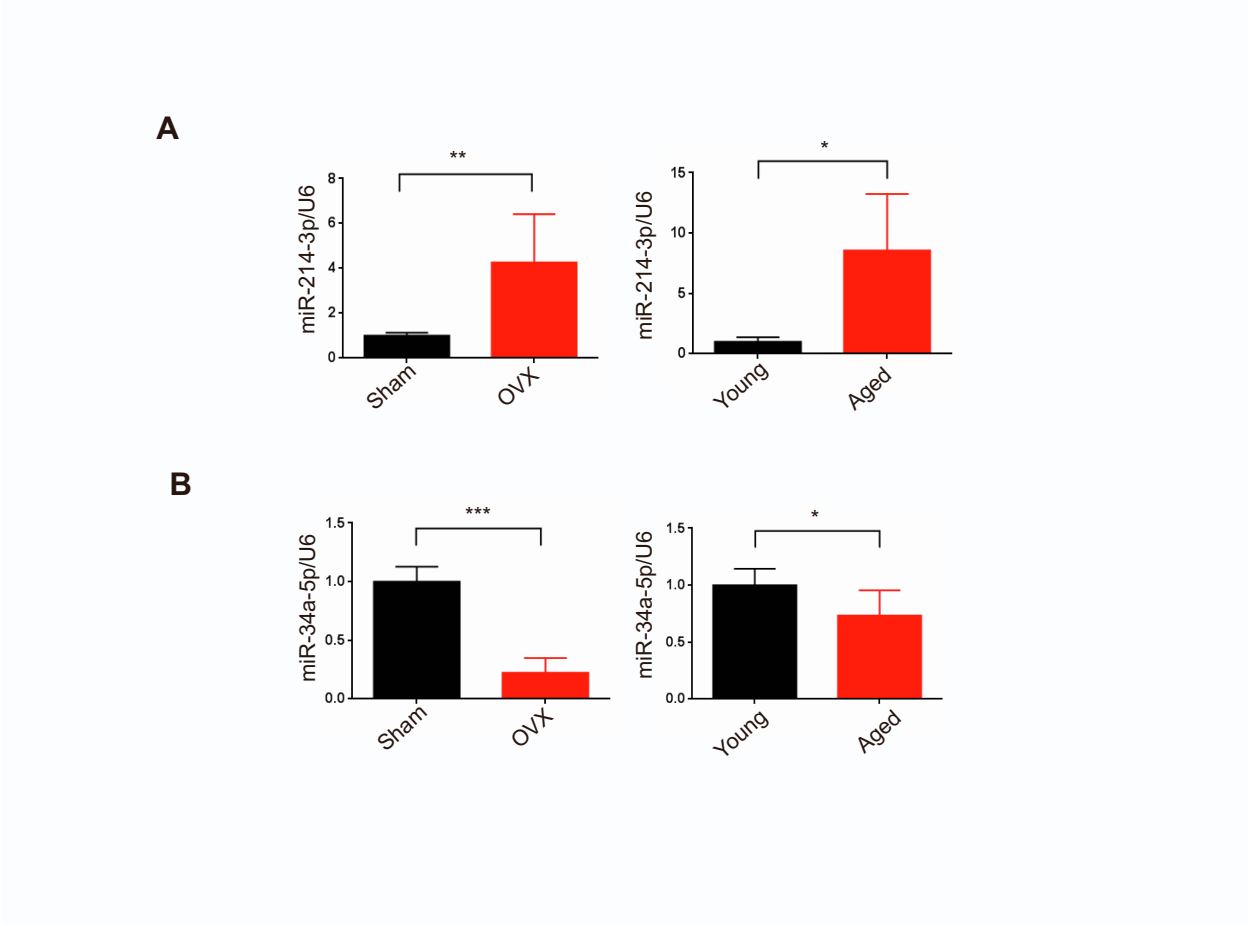

Supplementary Figure 1. **Expression of miR-214-3p and miR-34a-5p in osteoporotic bones.**

Expression of miR-214-3p (A) or miR-34a-5p (B) in the tibia of 16-week-old female mice with Sham or OVX surgery or 2.5-month-old (young) or 24-month-old (aged) male mice was assessed by RT-qPCR. Values represent mean ± SD: *P < 0.05; **P < 0.01; and ***P < 0.001 by an unpaired two-tailed Student's t-test.

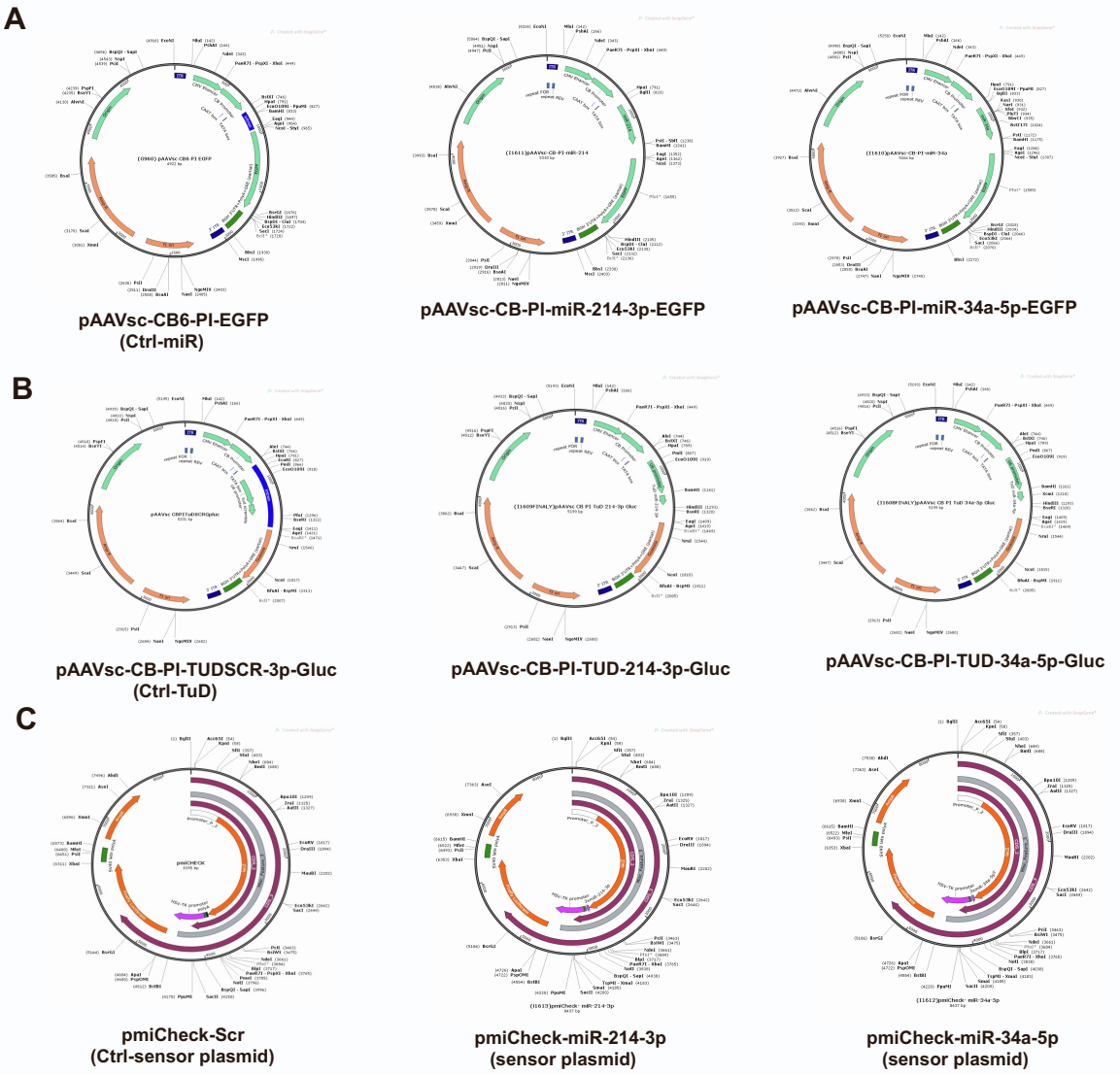

Supplementary Figure 2. Construction of AAV vector genomes and sensor plasmids.

(A) AAV vector genomes containing CBA (CMV enhancer/chicken β-actin) promoter, miRNA (miR-214-3p or miR-34a-5p), and the EGFP gene. (B) AAV vector genomes containing CBA promoter, tough decoy (miR-214-3p TuD or miR-34a-5p TuD), and the *Guassia* luciferase (gLuc) gene. (C) Sensor plasmids containing the complementary sequences of miR-214-3p or miR-34a-5p in the 3'-UTR of Lac Z (β-galactosidase) reporter gene.

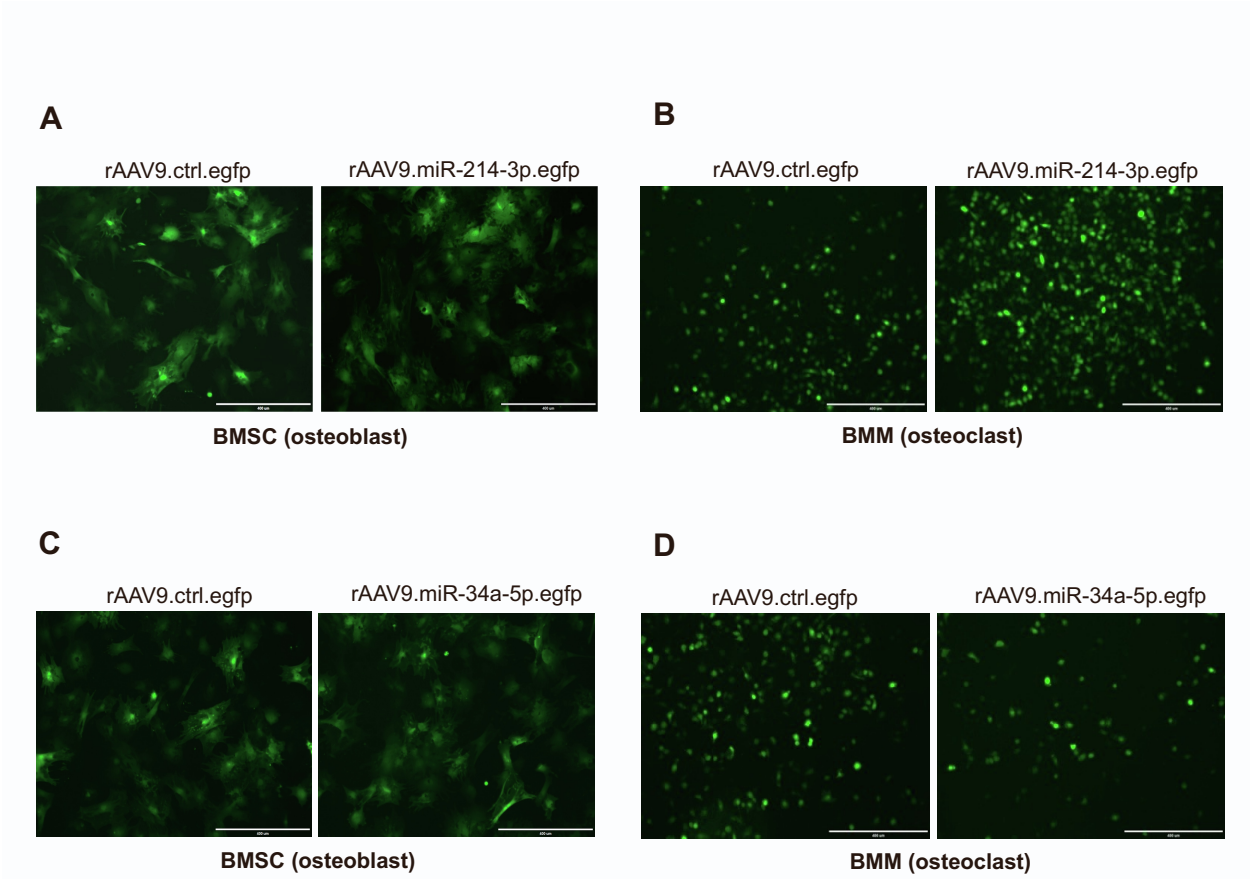

Supplementary Figure 3. *In vitro* transduction efficiency of rAAV9 vectors in the osteoblast and osteoclast.

(A, C) Mouse bone marrow-derived stromal cells (BMSCs) were incubated with rAAV9.egfp carrying ctrl, miR-214-3p or miR-34a-5p for two days and transduction efficiency was assessed by EGFP expression using fluorescence microscopy. (B, D) Two days after treatment with M-CSF and RANKL, mouse bone marrow-derived monocytes (BMMs) were incubated with rAAV9.egfp carrying ctrl, miR-214-3p or miR-34a-5p for two days and transduction efficiency was assessed by EGFP expression using fluorescence microscopy. Scale bars: 400 μm.

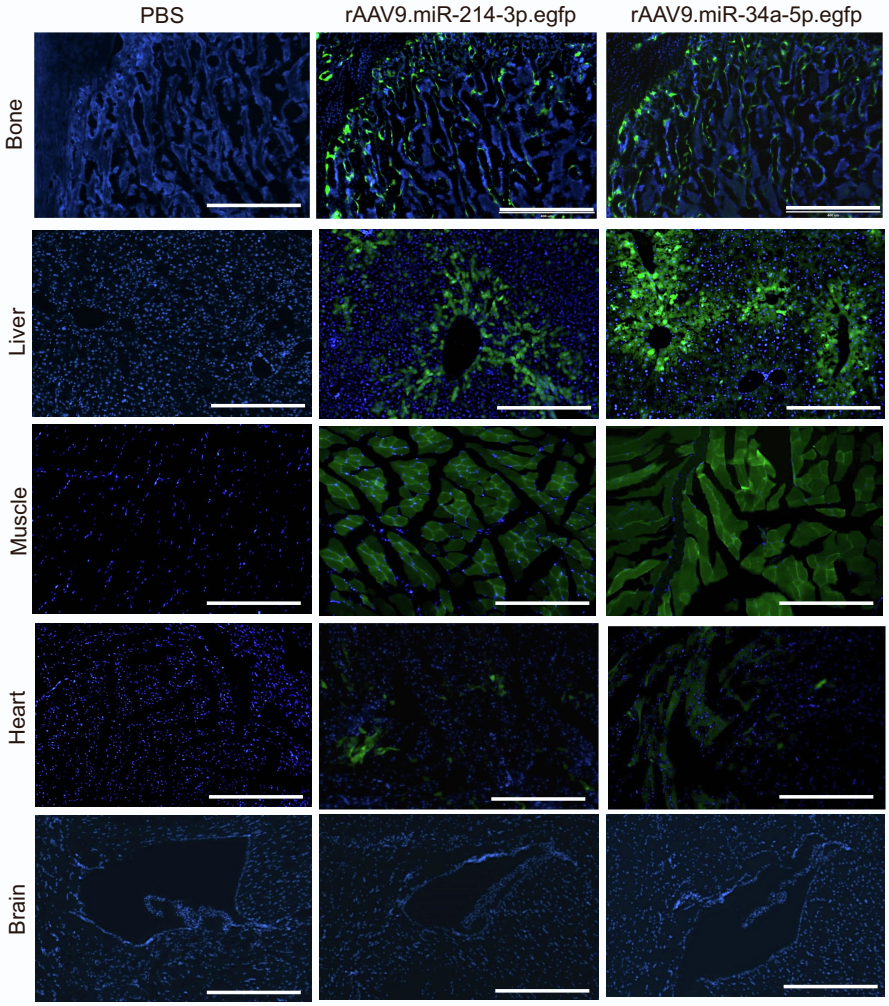

Supplementary 4. Tissue distribution of systemically delivered rAAV9 vectors in mice.

Two-month-old healthy mice were i.v. injected with a single dose of PBS or rAAV9 (5×10^{13} kg/vg) carrying ctrl, miR-214-3p, or miR-34a-5p, and two weeks later, EGFP expression in individual tissues was assessed by fluorescence microscopy. Scale bars: 400 μm.

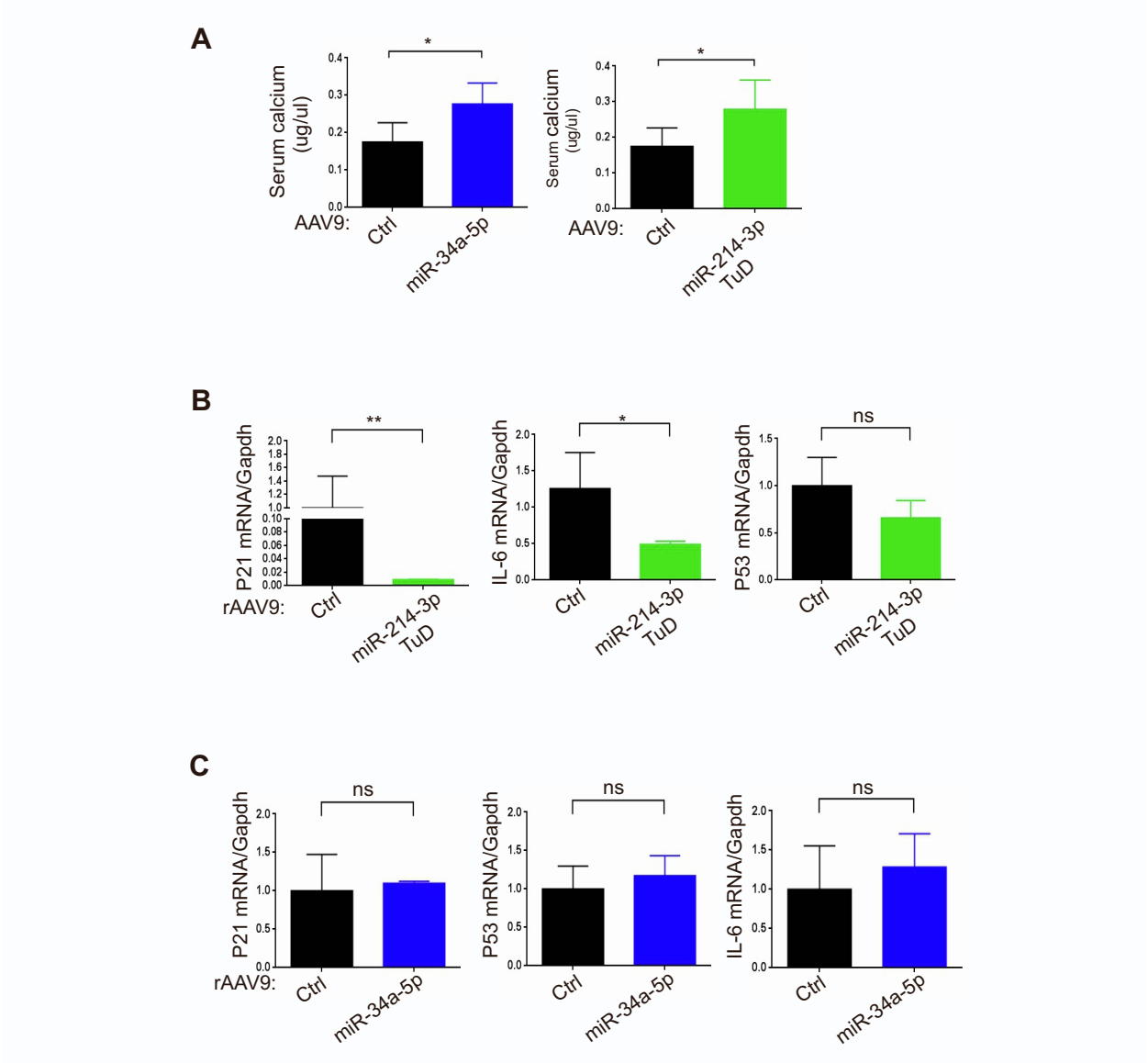

Supplementary Figure 5. Effects of AAV9 vectors carrying miR-214-3p TuD or miR-34a-5p on serum calcium levels and bone senescence in aged mice.

24-month-old male mice (n = 5) were i.v. injected with a single dose of rAAV9 (5×10^{13} kg/vg) carrying ctrl or miR-214-3p TuD or miR-34a-5p, and eight weeks later, calcium levels in the serum were measured by calorimetric assay (A). mRNA levels of cell senescence marker genes, including p21, p53, and IL-6, were assessed by RT-PCR analysis and normalized to Gapdh (B, C). Values represent mean ± SD: *P < 0.05; **P < 0.01; and ns, not significant by an unpaired two-tailed Student's t-test.

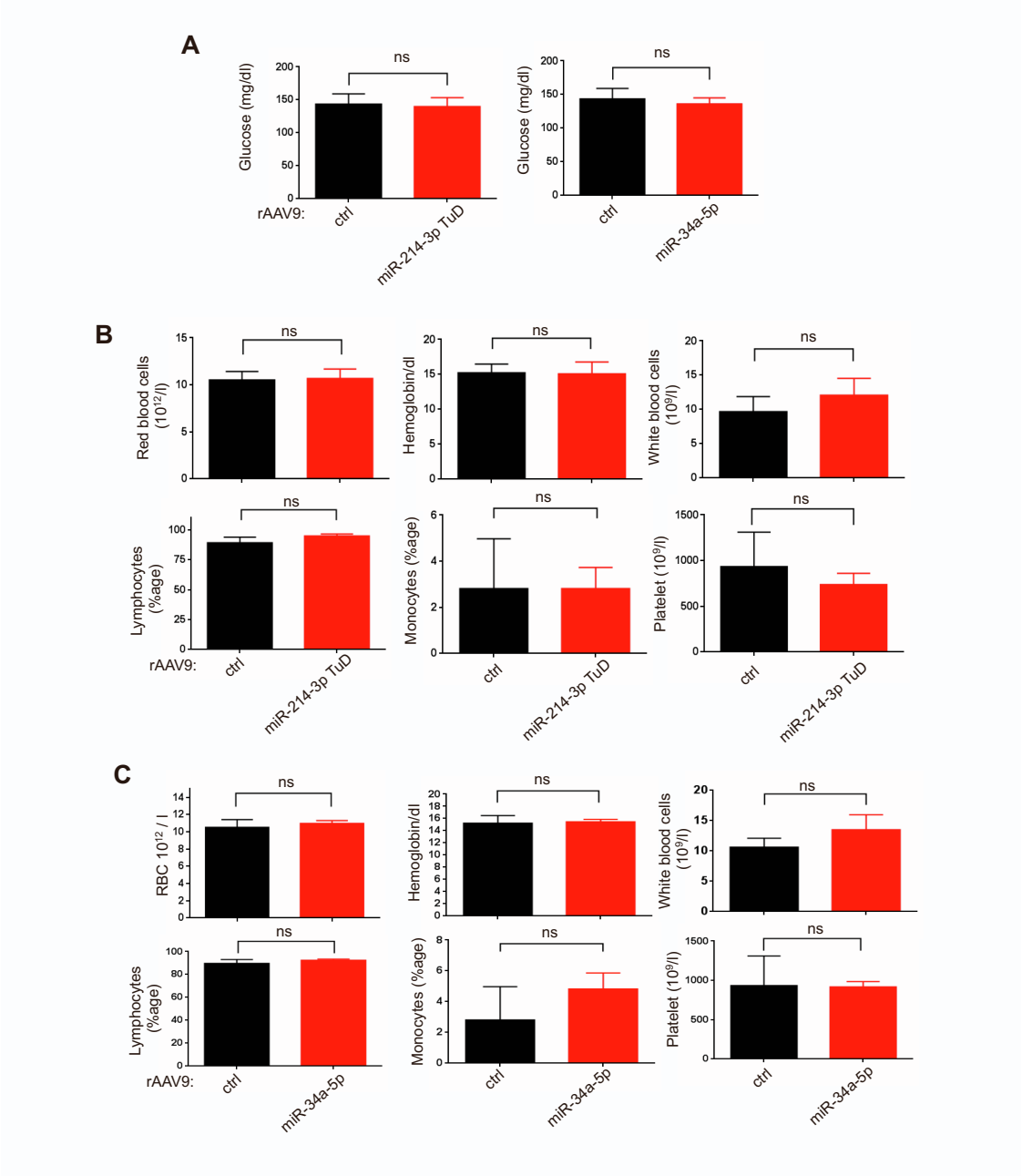

Supplementary Figure 6. Effects of AAV9 vectors carrying miR-214-3p TuD or miR-34a-5p in healthy mice.

Ten-week-old healthy mice were i.v. injected with a single dose of rAAV9 (5×10^{13} kg/vg) carrying ctrl, miR-214-3p TuD, or miR-34a-5p and eight weeks later, tests for blood glucose levels (A) and complete blood count (CBC) (B, C) were performed in AAV-treated mice (n = 5). Values represent mean ± SD: ns, not significant by an unpaired two-tailed Student's t-test.

Supplementary Table 1. Mouse primer sequences for RT-PCR

Name	Forward Primer	Reverse Primer
Runx2	TACAAACCATACCCAGTCCCTGTTT	AGTGCTCTAACCACAGTCCATGCA
Ibsp (Bsp)	CAGGGAGGCAGTGACTCTTC	AGTGTGGAAAGTGTGGCGTT
Sp7 (Osx)	ATGGCGTCCTCTCTGCTTGA	GAAGGGTGGGTAGTCATTTG
Bglap (Ocn)	GCAGCACAGGTCCTAAATAG	GGGCAATAAGGTAGTGAACAG
Pten	AATTCCCAGTCAGAGGCGCTATGT	GATTGCAAGTTCCGCCACTGAACA
Notch1	AACAGTGCCGAATGTGAGTGG	AAGTGACGCAAGAGCACCTAG
Atf4	ATGATGGCTTGGCCAGTG	CCATTTTCTCCAACATCCAATC
Tgif2	CCTCTCGGTGCTGCAGATA	TAGGGTCTTTGCCATCCTTC
Ctsk	AGCAGAACGGAGGCATTGACTC	CCCTCTGCATTTAGCTGCCTTTG
Acp5	GCGACCATTGTTAGCCACATACG	CGTTGATGTCGCACAGAGGGAT
RANK	TGGGTGATTTTCTTTTGGTGGG	CCAAGAACCAGTGCTCGTGA
Gapdh	ACTGAGCAAGAGAGGCCCTA	TATGGGGGTCTGGGATGGAA
Hprt	CTGGTGAAAAGGACCTCTCGAAG	CCAGTTTCACTAATGACACAAACG

Supplementary Table 2. Oligonucleotides and gBlocks used in this study

Oligonucleotides	Sequence(5′to3′)	Aims
TuD34a-5p F	CATCAACACAACCAGCTAAGTCGGACACTGCCACAAG TATTCTGGTCACAGAATACAACACAACCAGCTAAGTCG GACACTGCCACAAG	To generate TuD34a-5p for miR-34a-5p inhibition
TuD34a-5p R	TCATCTTGTGGCAGTGTCCGACTTAGCTGGTTGTGTTG TATTCTGTGACCAGAATACTTGTGGCAGTGTCCGACTT AGCTGGTTGTGTT	
TuDmiR-214-3P F	CATCAACACTGCCTGTCTGGTCGTGCCTGCTGTCAAGT ATTCTGGTCACAGAATACAACACTGCCTGTCTGGTCGT GCCTGCTGTCAAG	To generate TuD214-3p for miR-214-3p inhibition
TuDmiR-214-3P R	TCATCTTGACAGCAGGCACGACCAGACAGGCAGTGTT GTATTCTGTGACCAGAATACTTGACAGCAGGCACGAC CAGACAGGCAGTGTT	
3xmiR-34a-5pT sense	TCGAGACAACCAGCTAAGACACTGCCAACAACCAGCT AAGACACTGCCAACAACCAGCTAAGACACTGCCAGC	To generate miR-34a-5p targeting sites
3xmiR-34a-5pT antisense	GGCCGCTGGCAGTGTCTTAGCTGGTTGTTGGCAGTGT CTTAGCTGGTTGTTGGCAGTGTCTTAGCTGGTTGTC	
3xmiR-214-3p sense	TCGAGACTGCCTGTCTGTGCCTGCTGTACTGCCTGTCT GTGCCTGCTGTACTGCCTGTCTGTGCCTGCTGTGC	To generate miR-214-3p targeting sites
3xmiR-214-3p antisense	GGCCGCACAGCAGGCACAGACAGGCAGTACAGCAGG CACAGACAGGCAGTACAGCAGGCACAGACAGGCAGTC	
miR-34a gBlock	GTCTTTTATTTCAGGTCCCAGATCTTGGCTTCCAAGTG CTGGAGGAGTGTGTCATACCTCGGTAGGGTCCACTAC ACATCTTTCTCCCGCAGCCTCTCCATCTTCCTGTGACT GCGGGCGCCTCAGCCTGGGCTGGCCAGCTGTGAGTA ATTCTTTGGCAGTGTCTTAGCTGGTTGTTGTGAGTATT AGCTAAGGAAGCAATCAGCAAGTATACTGCCCTAGAA GTGCTGCACATTGTTGGGCCGAGAAGGAAAAGGTCAG AGGTCAGCAACGCCCACACCCCTGAGAGGCGCTGGA CTTGCGGAGCTGCTCGACCATACTGGTGGGTATGGGA TGCTGGGGAGGCTGGTGTTACTGCAGGGGATCCGGT GGTGGTGC	To express miR-34a-5p
miR-214 gBlock	GTCTTTTATTTCAGGTCCCAGATCTTTAGTTCCATAATG TTTTAATGTTTAATTCTATTGTGTGTTTCTCTCCTTTCCC TTTATCCCCCTGTCCTTCCCCCCTAAATCACCAAATCT GGAAAACAGGCTGATTGTATCTGTCCCTGAGCAAAGG AAACCTGAAGGACCCAAGGGCCTGGCTGGACAGAGTT GTCATGTGTCTGCCTGTCTACACTTGCTGTGCAGAACA TCCGCTCACCTGTACAGCAGGCACAGACAGGCAGTCA CATGACAACCCAGCCTGAATGACCACCAGCCATTGAA AGAAAGCTGCCCTCACAACATAGCATCTACACCAAGAG CTACAACCACAGTGAGGGGGTTGGGGGGCCTGGGGT TTGAAACTGTTGGCTTATTAAAAGAAAAACTCGTATGTA ATCCCTGCAGGGGATCCGGTGGTGGTGC	To express miR-214-3p